A THESIS FOR THE DEGREE OF MASTER OF SCIENCE

A Study on the High Breakdown Voltage AlGaN/GaN HEMTs Employing H_2O Annealing and HfO_2 Gate Insulator

수증기 어닐링과 HfO_2 게이트 절연막을 적용한 고전압 AlGaN/GaN HEMTs 에 관한 연구

by

Woojin Ahn

August 2013

Department of Electrical and Computer Engineering
College of Engineering
Seoul National University

Abstract

A Study on High Breakdown Voltage AlGaN/GaN HEMTs Employing H_2O Annealing and HfO_2 Gate Insulator

Woojin Ahn

Department of Electrical Engineering and Computer Science

College of Engineering

Seoul National University

AlGaN/GaN high-electron-mobility transistors (HEMTs) have received a considerable amount of attention for high-power application such as RF and power electronic systems due to their wide bandgap properties, such as their high critical field (3 MV/cm) and low intrinsic carrier concentration (10^{10} cm^{-3}). Also, AlGaN/GaN heterostructure offers a high density (10^{13} cm^{-2}) and a high mobility (2000 $cm^2/V{\cdot}s$) for a two-dimensional electron gas such that AlGaN/GaN HEMTs exhibit a high breakdown voltage with a low on-resistance.

However, the soft breakdown characteristic of AlGaN/GaN HEMTs caused by surface leakage current is a critical issue. AlGaN/GaN HEMTs have a considerable amount of surface states such as that related to

dislocation from the GaN buffer/substrate interface, arranged charges caused by spontaneous polarization charges, and nitrogen vacancies induced by plasma and thermal processes. At a high breakdown voltage, the electron trapping at shallow traps on the surface should be suppressed.

In order to improve the reverse blocking characteristics of AlGaN/GaN HEMTs, I fabricated AlGaN/GaN HEMTs employing the proposed H_2O annealing treatment and compared electrical characteristics with those of the HEMT by widely used O_2 annealing method. The breakdown voltage and the drain leakage current of AlGaN/GaN HEMT (L_{GD}= 20 μm) employing the H_2O annealing treatment were 1674 V and 13.1 nA/mm (V_{DS}= 100 V, V_{GS}= –10 V), respectively, while those of HEMT with the O_2 treatment were 1512 V and 60.1 nA/mm.

Not only relatively degraded reverse blocking characteristic but also a normally-on characteristic of AlGaN/GaN HEMTs has been dealt as a serious issue. Most of previously reported AlGaN/GaN HEMTs have a normally-on characteristic with threshold voltage (V_{TH}) of –3 to –6 V due to the polarization-induced 2DEG between AlGaN and GaN layer. In order to prevent 'Burn-out' phenomenon and designing additional circuit because of the normally-on devices, normally-off characteristic is strongly desirable for an integrated circuits application.

In this thesis, by applying simple KOH wet etch and RF-sputtered HfO_2 as a gate insulator, normally-off AlGaN/GaN MOS HEMTs were successfully fabricated and investigated. The proposed KOH wet etch resulted in an adequate recess-depth and smooth etched surface. The gate-recessed HEMT exhibits threshold voltage (V_{TH}) shifts from –3 to 1.5 V after 150 s KOH-wet etch. The breakdown voltage of 1580 V and

specific on-resistance ($R_{on,sp}$) of 8.09 mΩ·cm^2 was measured in AlGaN/GaN HEMT with the gate-drain distance of 20 μm-long. The high figure of merit (FOM) of 308 MW·cm^{-2} was achieved. My experimental results indicate that the proposed simple KOH wet etching and RF sputtered HfO_2-gate insulator may be promising for the normally-off AlGaN/GaN MOS HEMTs fabrication.

Lastly, another recent issue of AlGaN/GaN HEMT is dealt in the Appendix chapter which is a gold free issue. Conventional conducting metal Ni/Au was compared with Ni/Cu and Ni/W contact. My experimental result shows that Cu also may be a good conducting metal for AlGaN/GaN HEMTs and has a great potential for power device application. Moreover, I have proposed and fabricated high performance of AlGaN/GaN Schottky Barrier Diodes (SBDs) with various Schottky contact by sputtering method. The reverse blocking characteristics such as the leakage current and breakdown voltage was improved by TaN and ITO Schottky contact due to its high SBH. However, forward current of TaN and ITO Schottky contact was less than that of Ni/Au Schottky contact. The TaN Schottky SBDs achieved the highest breakdown voltage of 605 V and ITO Schottky SBDs achieved 472 V. On the contrary, the breakdown voltage of Ni/Au Schottky SBDs exhibited 335 V.

Keywords: GaN, AlGaN, Normally-off, High-Electron-Mobility Transistors, H_2O annealing, HfO_2, KOH wet etching

Student Number: 2011-23366

Contents

List of Figures and Tables

Chapter 1

1. Introduction

1.1. Background

The market of power semiconductor devices grows bigger and bigger as time passes. Even though the market depressed in the year 2009 due to world-wide business slack, now the market is rising abruptly by power module demand which belongs to hybrid vehicles, electrical vehicles, and new renewable energy system. An ideal electronic system requires high conversion efficiency, low power loss, compact size, and these three requirements can be realized by high-performance power semiconductor devices which exhibit high breakdown voltage, low on-resistance and thermal stability.

Silicon power devices have been vastly studied due to its many advantages such as abundance, low-cost, ease in oxidization and low impurity density. However, Si-based semiconductor device technology has

reached its limit due to silicon's physical and material properties. Many researchers have tried to find alternative materials that can get over Si-limitation and finally they found wide band-gap materials such as GaAs, GaN, and SiC [1]. Figure 1-1 shows the comparison of R_{on} and for Si, SiC, and GaN [2]. Figure 1-1 indicates that the necessity of wide band-gap based power devices in order to obtain high power density and high conversion efficiency for more advanced electronic and power system.

Material's energy band-gap, temperature and doping concentration determines critical electric field of a certain material and it directly relates to the avalanche breakdown voltage. Above all, band-gap affects critical-electric-field the most since this value increases proportionally to the band-gap value by power of 2.5. Therefore, wide band-gap devices can sustain higher breakdown voltage when it compared with the same size of silicon devices [3]. In other words, wide band-gap devices can sustain same breakdown voltage as much as bigger Si-based devices. Moreover, low intrinsic carrier concentration and low probability of band-to-band emission characteristic of wide band-gap materials enable the efficient power conversion and high temperature operation without large-sized cooling system. The theoretical properties of various semiconductor materials are summarized in Table 1-1 [3, 4, 5]. As you can see in Table, GaN has high critical electric field, high electron mobility, and high saturation velocity compared with Si, GaAs, and SiC. Therefore, GaN is a promising and a suitable material for future high power systems such as electric vehicle, hybrid vehicle, and renewable energy power module [6, 7].

As growth and deposition technique develops, SiC began to receive attention from good thermal characteristics and chemical stability. As a

result, SiC Schottky Barrier Diodes (SBDs) are commercialized recently. Moreover, SiC-based metal-oxide-semiconductor field-effect-transistors (MOSFETs) and insulated gate bipolar transistors (IGBTs) have been developed as well. However, the difficulty of making large wafer and high cost for the fabrication make prospects of SiC-based power devices still questionable.

Also, the diamond has been regarded as a promising material for the next-generation power semiconductors' material due to its superior material properties. However, diamond also has the problems of impurity doping and deep-carrier activation energy. Diamond's difficult fabrication issue must be solved in order to be employed to the power semiconductor [8].

In 1965, Johnson derived the following figure of merits (FOMs) formula in order to compare each material-limitation.

$$\text{Johnson's FOM} = \left(\frac{E_c V_{sat}}{\pi} \right)^2$$

E_c and V_{sat} are the critical field and the saturation velocity, respectively [9]. In the Johnson's FOM formula, the critical field and the saturation velocity is the main factors which limit the performance of typical devices.

In 1982, Baliga derived new FOM formula for power FETs. This FOM formula is to minimize the conduction loss in power FETs [10]. The ε, μ, and E_G are permittivity, mobility and energy gap of semiconductor materials, respectively.

$$\text{Baliga's FOM} = \varepsilon \cdot \mu \cdot E_G^3$$

Baliga's FOM is based upon the assumption that the power dissipation of devices is originated from the only current flow through channel. The calculated values for Si, GaAs, SiC, and GaN are summarized in Fig. 1-2. As shown in Fig. 1-2, GaN has the highest values compared with other semiconductor materials in both Baliga's and Johnson's FOM so that GaN-based semiconductors are suitable for the future power system.

However, this promising GaN has several obstacles to be commercialized as a device such as MOSFETs or IGBTs due to its material limitation. Of all the most, p-type doping is a crucial obstacle to overcome. Still, despite of many researchers' efforts to solve these issues, successful fabrication and operation have been demonstrated scarcely. The most widely employed method for p-GaN growth is adding Mg-based mixture during GaN growth. By this method, the maximum hole concentration that can be achieved is about 10^{19} cm^{-3} which is quite low value. This low value of the concentration is attributed the high activation energy and very low activation ratio. As a result, the resistance of p-GaN is high compared with n-GaN and this causes a considerable voltage drop across PN or PiN junction. Also, the hole mobility of p-GaN is low as 10 $cm^2/V{\cdot}s$ so that GaN-based high-performance bipolar devices are difficult to fabricate [3].

Thus, high-electron-mobility transistors (HEMTs) and Schottky barrier diodes (SBDs) fabricated on the hetero-structure of AlGaN and GaN has been studied widely and many results have been reported. Many merits of AlGaN/GaN HEMTs is attributed by a highly conductive channel so called two-dimensional electron gas (2DEG) which is induced by

polarization effect at the interface between AlGaN and GaN layer [11]. 2DEG exhibits high sheet charge density, electron mobility, and saturation velocity without any doping process [11, 12]. With these features, the hetero-structure of AlGaN/GaN HEMTs also shows high critical electric field characteristic which enables high voltage operation with low static and dynamic power loss.

However, AlGaN/GaN HEMTs also have several issues. First of all, lack of the native GaN substrate is a critical issue. Thus, at present, GaN layer is widely grown on Sapphire, SiC, and Si. As a result, the mismatch in lattice and thermal coefficient between substrate and GaN induces considerable dislocations and defects in the GaN epitaxial layer [13]. These factors affect device-performance badly. Mismatches of lattice and thermal coefficient between GaN and substrate are summarized in Table 1-2 [13].

As shown in Table 1-2, SiC shows the smallest mismatches in lattice and thermal coefficient with GaN so that low dislocation density and high devices performance are expected. However, only a few companies have produced SiC substrate because of the expensive cost to produce so that this material is undesirable for the mass-production. Moreover, the maximum reported wafer size is less than 6 inches up to now. On the contrary, sapphire is relatively cheaper than SiC. Also, sapphire exhibits smaller mismatch than Si. However, the low thermal conductivity characteristic may induce a large self-heating effect which is a detrimental factor to the forward electrical characteristics of AlGaN/GaN HEMTs. When Si is compared with SiC and sapphire substrate, Si is a very promising material for AlGaN/GaN HEMTs substrate due to its low cost. For instance, the 14 inch Si wafer is commercially available now. However,

large lattice mismatch with GaN is the issue which may causes serious dislocation and wafer bowing problems. This lattice mismatch issue and wafer bowing issue have been compensated well by recent developed growth technology and thick Si substrate over 1 mm.

As a result, based on the excellent material characteristics of GaN, high-performance GaN power devices have been demonstrated recently as shown in Fig. 1-3. The company Transphorm has released GaN-on-Si transistor which is qualified by the joint electron device engineering council (JEDEC) standard [14]. Also, IMEC has reported 8 inch Au-free AlGaN/GaN MOS-HEMT-on-Si using Cu-based electrodes [15]. Moreover, vertical diodes with breakdown voltages up to 2.6 *k*V have been fabricated on bulk GaN substrates [16]. These devices show performance near the theoretical limit of GaN.

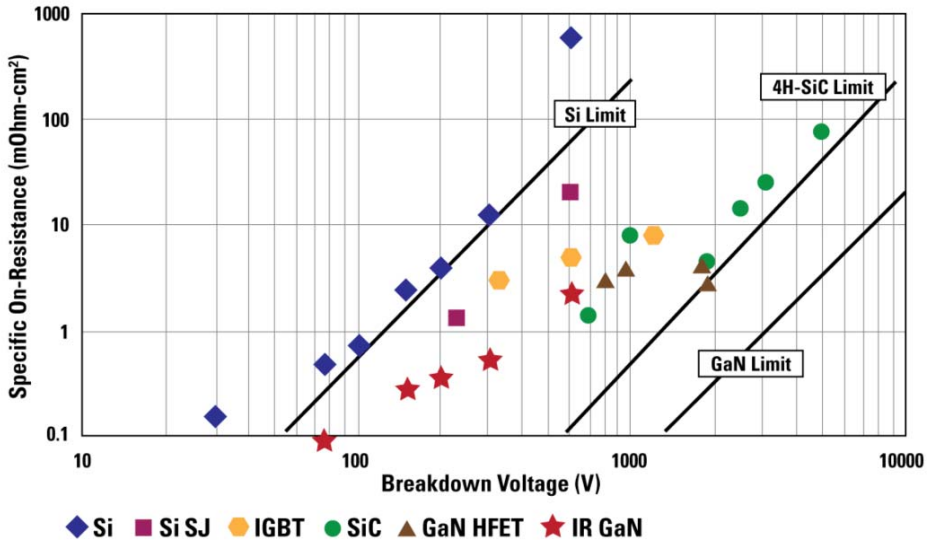

Figure 1-1: Silicon-limitation and potential of GaN power devices [2].

Table 1-1: Material properties of semiconductors [3, 4, 5]

		Si	GaAs	GaN	SiC		Diamond
					4H	6H	
Bandgap at 300 ^{o}C (eV)		1.12 Indirect	1.42 Indirect	3.44 Direct	3.25 Indirect	2.86 Indirect	5.46-5.60 Indirect
Bulk mobility at 300 K (cm^2/Vs)	Electron	1400	8500	900	700	330-400	2200
	Hole	450	400	10	NA	75	1800
Saturation velocity (10^7 cm/s)		1	2	2.5	2	2	3
Critical field (10^6 V/cm)		0.3	0.4	3.5	3.2	2.4	7
Thermal conductivity (W/cmK)		1.3	0.55	1.1	4	5	6-20

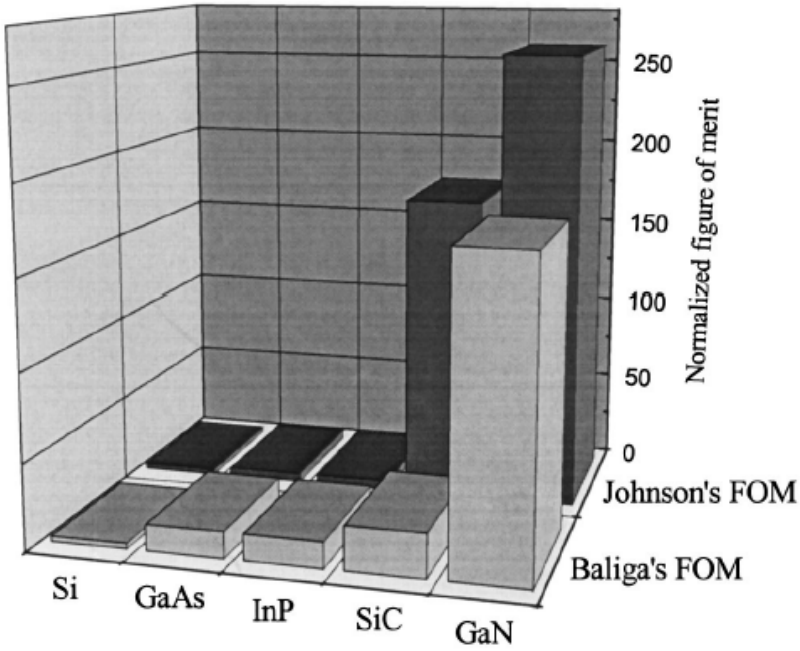

Figure 1-2: Baliga's and Johnson's figure of merit (FOM) for various semiconductors [4].

Table 1-2: Crystal and thermal properties of various substrates [13]

	Lattice constant (Å)	Typical growth plane	Lattice mismatch with GaN	Thermal expansion coefficient
6H-SiC	a=3.081 c=5.7034	(0001)	3.51 %	a=4.2 c=4.68
Sapphire	a=4.765 c=12.982	(0001)	13.9 %	a=7.5 c=8.5
Si	A=5.431	(111)	–16.96 %	3.9

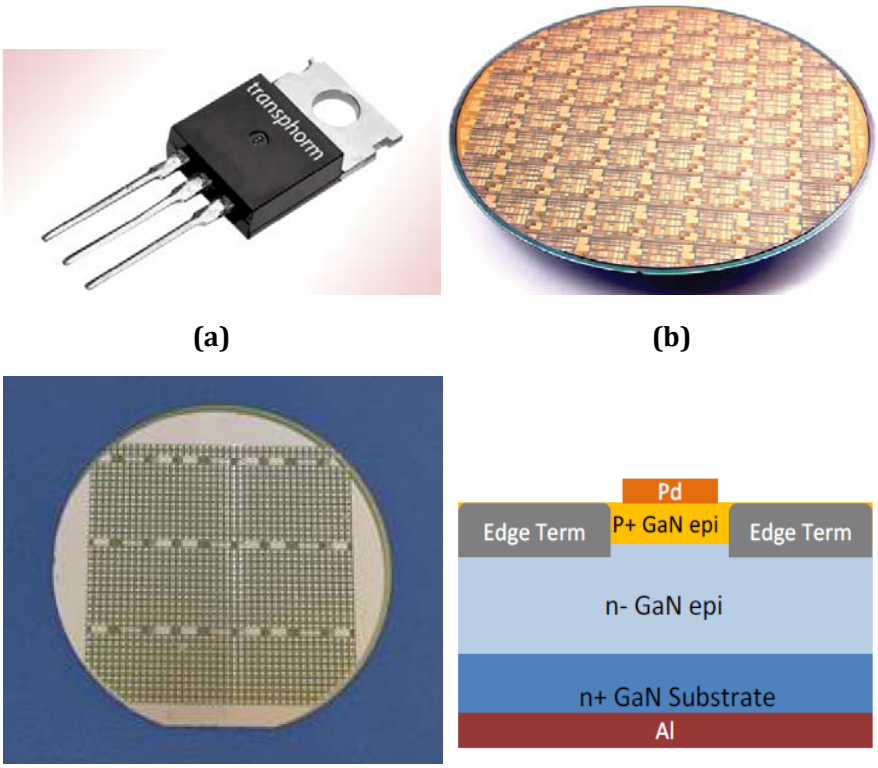

Figure 1-3: Demonstrated GaN power devices **(a)** JEDEC-qualified 600 V GaN-on-Si device **(b)** 8 inch GaN-on-Si MIS-HEMT device **(c, d)** Vertical power diodes in bulk GaN [14, 15, 16].

1.2. Outline of this thesis

In this thesis, I proposed and investigated two methods for the high-performance AlGaN/GaN HEMTs, H_2O annealing and RF-sputterd HfO_2 gate insulator.

Chapter 2 describes the overview of AlGaN/GaN HEMTs. The basic structure, fabrication processes, operation principle, key issues limiting the electrical properties of the device, and recent studies to improve device performance by using RF-sputtered gate insulator HfO_2 are reviewed.

Chapter 3 introduces H_2O annealing for AlGaN/GaN MOS-HEMTs to enhance reverse blocking characteristic. At first, device fabrication processes and the structure are described in chapter 3.2. Secondly, in order to investigate the effects of H_2O annealing on the surface, XPS and AES measurement are dealt in chapter 3.3. At last, various experimental results, reverse blocking characteristics, DC *I-V* characteristics, and pulsed *I-V* are described and discussed in chapter 3.4.

Chapter 4 describes KOH wet etching technique and RF-sputtered HfO_2 for the normally-off AlGaN/GaN MOS HEMTs. Firstly, in chapter 4.2, device fabrication processes and the structure is introduced. Secondly, the result of KOH wet etching is exhibited in chapter 4.3. Lastly, various electrical results of AlGaN/GaN MOS HEMTs is discussed in chapter 4.4.

My works and future works are summarized in chapter 5. Lastly, in appendix, another important issue of AlGaN/GaN HEMT which is the gold free issue is been dealt and related experiments are described.

Chapter 2

2. Review of AlGaN/GaN Power Devices

In this chapter, more detailed characteristics of AlGaN/GaN HEMT are reviewed. First section introduces AlGaN/GaN HEMTs' operation principles, structure, and fabrication. Second section deals with two major issues of AlGaN/GaN HEMT which are directly related with the overall contents of this thesis. First issue is surface state issue and the other issue is normally-on issue. Last section introduces about RF-sputterd HfO_2 for gate insulator.

2.1. Device Structure, Operation, and Fabrication

Figure 2-1 shows the structure and the operation of AlGaN/GaN HEMT. AlGaN and GaN are commonly grown on the Si substrate by

chemical vapor deposition method. Current of the device runs through highly conductive channel so called two dimensional gas (2DEG) which is located at the interface between AlGaN and GaN layer. The formation of 2DEG is caused by the spontaneous and the piezoelectric polarization at the interface between AlGaN and GaN layer as shown in Fig. 2-2 [12, 25]. Piezoelectric polarization in the case of AlGaN/GaN HEMT, is generally caused by the lattice constant difference between AlGaN and GaN. Also, the specific structure of GaN which is Wurtzite crystal structure is the main reason for the formation of piezoelectric polarization effect.

Also, the concentration of 2DEG changes according to the thickness of AlGaN layer and the mole fraction of Al [12]. Higher Al composition in AlGaN barrier results in larger band discontinuity so that the improvement of carrier confinement, strong piezoelectric polarization, high sheet charge and highly composite breakdown field can be realized [5]. However, high Al composition restricts the critical thickness of AlGaN due to the large lattice mismatch at AlGaN/GaN interface. Moreover, the high Al composition increases the ohmic contact resistance. In order to achieve low ohmice contact resistance, one group reported re-grown AlGaN layer [17]. Therefore, AlGaN barrier layer should be optimized for its applications.

As shown in Figure 2-1, the operation of AlGaN/GaN HEMT is controlled by the bias of the gate electrode. When the gate voltage is higher than the threshold voltage, AlGaN/GaN HEMT is on-state. In this state, current flows from drain to source through highly conductive 2DEG. Generally, the threshold voltage of conventional AlGaN/GaN HEMT is less than 0 V by high-electron density due to the polarization effect. If the gate voltage is lower than the threshold voltage, current does not flow since

the channel between the source and the drain is blocked by the extended depletion region under the gate. The Schottky contact of gate electrode expands the depletion region if the applied voltage is less than the threshold voltage. In this off state, the leakage current induced by the surface state on the GaN may be an important issue of AlGaN/GaN HEMTs. The detail description of the surface leakage current is described in later section.

The major fabrication processes of AlGaN/GaN HEMT are mesa isolation, Ohmic contact formation, Schottky contact formation, and passivation. The mesa isolation process is to define the active region of AlGaN/GaN HEMTs and this process is generally done by the etching of AlGaN barrier layer and the GaN buffer layer. The etch-depth should be deeper than the location of 2DEG channel. By mesa isolation etching, the buffer leakage current flows between source and drain in off state may be induced by etching damage and it should be suppressed for the high-performance AlGaN/GaN HEMT.

The ohmic contact is to form electrodes such as source and drain by native oxide removal, e-gun evaporation, lift-off, and annealing process. Native oxide increases the ohmic contact resistance so that it should be removed using HCl or HF solution. The next step is Ti/Al based metals such as Ti/Al/Ni/Au, Ti/Al/Ti/Au, and Ti/Al/Mo/Au deposition by e-gun evaporator. The pattern of the ohmic contact is determined by the lift-off process. Lastly, the ohmic contact should be annealed in order to decrease the contact resistance mostly by rapid thermal annealing (RTA) at 800~900 ^{o}C under nitrogen ambient. The mechanism of ohmic contact is a formation of TiN which partially remove nitrogen vacancies on the GaN surface and direct connection between 2DEG channel and ohmic metals

[18]. Two layers on the Ti/Al layer is to suppress an oxidation of Ti/Al and to improve the conductivity of ohmic contact.

The next step is Schottky contact formation generally for the gate electrode. This process also composed of several sequence steps such as native oxide removal, metal deposition by e-gun evaporator, and lift-off. The deposited metal on the GaN surface determines the Schottky barrier height of the device and metals on the first deposited metal are for the prevention of the oxidation phenomenon. The value of the Schottky barrier height is equals to the difference between the work function of the metal and the GaN electron affinity (4.1 eV). High Schottky barrier height is desired for the small level of the leakage current induced by the tunneling. As a result, post annealing process under nitrogen or oxygen ambient was proposed by several groups [19, 20].

The last process is the passivation process. A variety of passivation processes have been introduced by many groups such as additional material deposition by many methods [21, 22, 23, 24]. More detail mechanism of the deposition of additional material is discussed in following chapters. The main purpose of the passivation is to suppress surface state on the GaN surface. The reasons for the surface states suppression is described in next section 2.2. Except for these two methods, field plate design of AlGaN/GaN HEMT is also widely known for the good reverse blocking characteristic device. The breakdown phenomenon occurs when the electric field converges too much at the gate edge. However, by extending the gate electrode to the drain side on the passivation layer, electric field crowding can be decreased so that the breakdown voltage may increase [21]. Despite of this merit, adding additional field plate structure requires one more photo-mask and

metallization process. Figure 2-3 shows fabrication processes of AlGaN/GaN HEMT employing gate-field plate based on the explanations above.

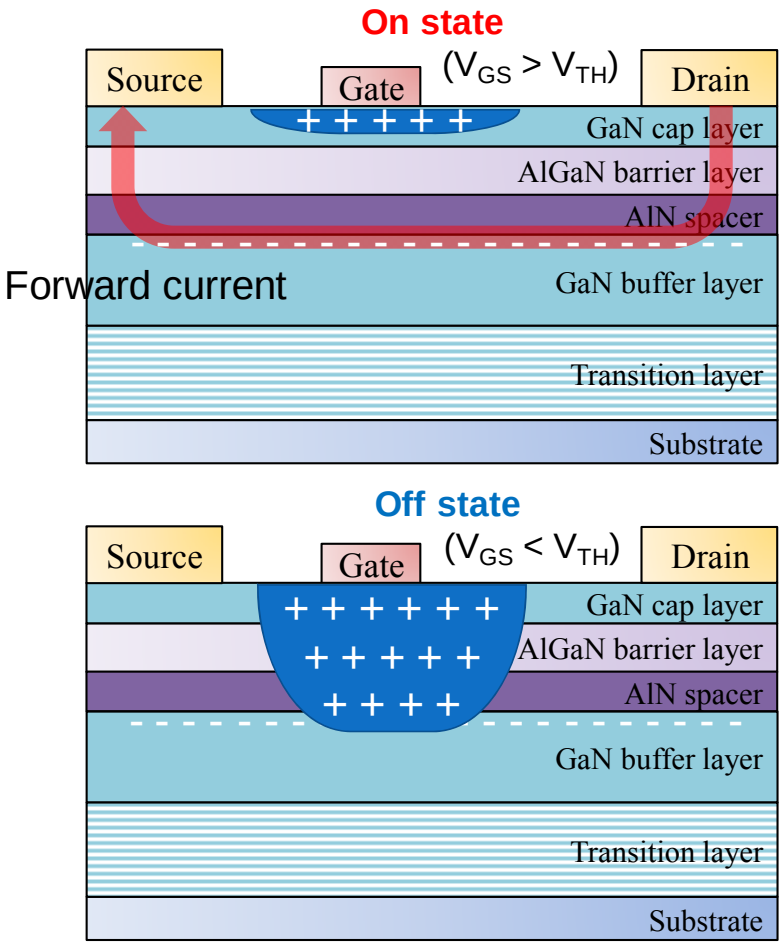

Figure 2-1: The structure and the operation of AlGaN/GaN HEMTs

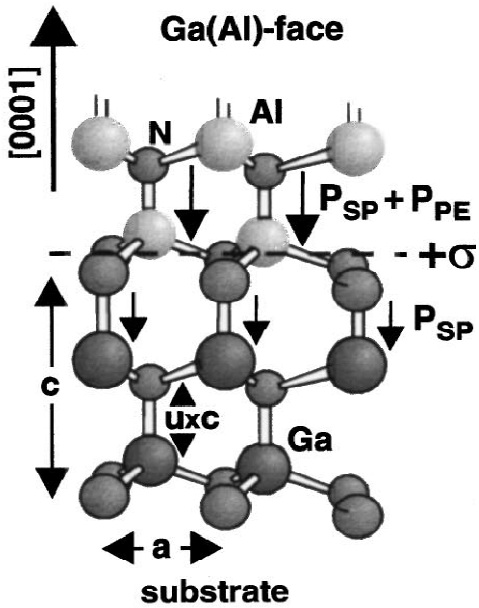

(a)

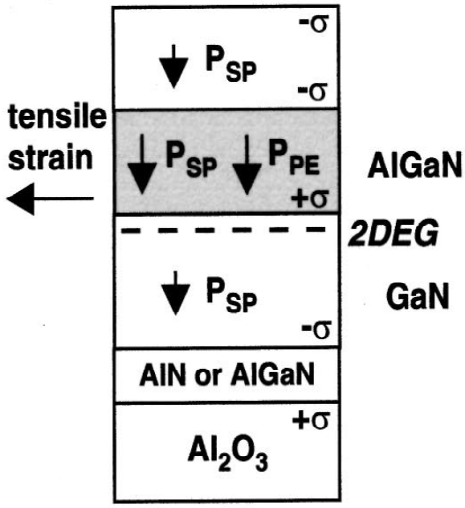

(b)

Figure 2-2: Ga (Al)-face AlGaN/GaN **(a)** crystal structure **(b)** polarization induced bound sheet charge, piezoelectric and spontaneous polarization [25].

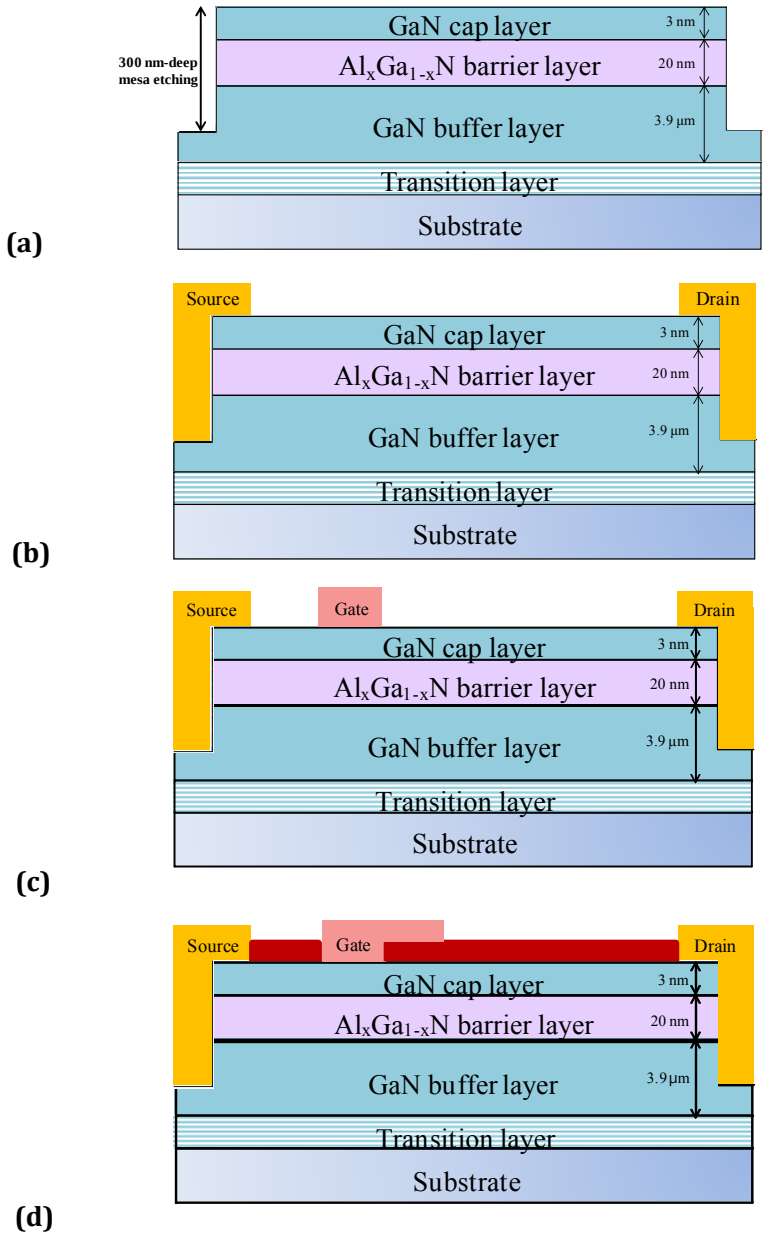

Figure 2-3: Fabrication process; **(a)** mesa etch, **(b)** Ohmic contact, **(c)** Schottky contact, **(d)** Passivation and gate field plate

2.2. Key Issues of AlGaN/GaN HEMTs

Even though AlGaN/GaN HEMTs have attracted considerable attention for its high voltage, high temperature, and high speed switching characteristics, still many issues need to be solved in order to be employed to power system. In this thesis, two main issues are dealt and the first topic is surface state issue and the other one is normally-off characteristic of AlGaN/GaN HEMTs.

2.2.1. Surface state issue

One of key issues of AlGaN/GaN HEMT is the surface state which occurs at the device surface. The surface state on GaN HEMT is too important to be neglected since it is the major reason for the surface leakage current during reverse operation. Considerable leakage current during the reverse operation will decrease the current on and off ratio of the device, additional power consumption at off state and breakdown voltage decrease, which are very detrimental for good device performance [26].

The reason for this surface leakage current is a considerable amount of surface states such as that related to dislocation from GaN buffer/substrate interface, arranged charges caused by spontaneous polarization charges, and nitrogen vacancies induced by plasma and thermal processes [11, 12]. At a high reverse voltage, the electron trapping at shallow traps on the surface degrades the performance of the device. Trapped electrons at shallow traps on the surface will emit to the

conduction band by room temperature thermal energy. Those electrons either flow through 2DEG at AlGaN/GaN interface by polarization effect or move to another trap at the drain side so called electron hopping phenomenon will occur. Trapping to shallow traps at the surface will induce the leakage current, furthermore, in the case of switching operation, it disrupts the current flow as you can see in Fig. 2-4 [27]. By this phenomenon occurring by electrons trapping at shallow traps, the length of the effective gate will expand and this gate is known as a virtual gate. This virtual gate phenomenon decreases the length of the space between the gate and the drain as the length of virtual gate increases. Eventually, reduced length of the space between the gate and the drain causes the breakdown voltage decrease so that the performance of the device is degraded.

In order to improve the reverse blocking characteristics of AlGaN/GaN HEMTs, various methods such as surface passivation employing Si_3N_4 [21], SiO_2 [22], BCB [23], Al_2O_3, and AlN have been reported. Also, an edge termination structure which includes a field plate [28], a floating metal [29], and a lightly doped drain using a fluorine treatment [30] have also been reported to improve the reverse blocking characteristics.

2.2.2. Normally-on issue

Another important issue of AlGaN/GaN HEMT is normally-on characteristic. V_{TH} of conventional AlGaN/GaN HEMT is known to be about –4 V which is less than 0 V. If we apply normally-on device to the high voltage switching system, burn-out phenomenon may occur even

when the gate electrode is grounded [31]. In order to alleviate this problem, we need extra circuit design so that many researches for the normally-off AlGaN/GaN HEMT fabrication are now ongoing.

Gate recessed structure is one of widely known techniques for the normally-off AlGaN/GaN HEMT fabrication. Figure 2-5 shows the structure of gate-recessed AlGaN/GaN HEMT for normally-off operation. As shown in Figure 2-5, AlGaN layer under the gate region is partially etched in order to remove the channel so that the V_{TH} of the device shifts to near 0 V. Especially, the etched-depth should be larger than the critical thickness of AlGaN layer which is the specific thickness of the 2DEG induction. The formula between sheet charge and the thickness of AlGaN layer is as follows.

$$n_s\left(d_g\right) = \frac{\sigma_{pol}}{e} - \frac{\epsilon_0 \epsilon_r}{e^2 d_g}\left(e\Phi_b + \Delta - \Delta E_0\right)$$

σ_{pol}, ϵ_0, ϵ_r, Φ_b, and ΔE_0 refer to sheet charge by the polarization, vacuum dielectric constant, dielectric constant of AlGaN, Schottky barrier height at the surface, and conduction energy band gap difference at AlGaN/GaN interface, respectively. Especially, Δ stands for following formula.

$$\Delta = E_0 + \frac{\pi\hbar}{m^*} n_s\left(d_g\right),\ \ E_0 = \left[\frac{9\pi\hbar e^2}{8\epsilon_0\sqrt{8m^*}} \frac{n_s\left(d_g\right)}{\epsilon_r}\right]^{\frac{2}{3}}$$

$\hbar$ and m^* refer to the plank constant and effective mass, respectively. Also, the sheet charge σ_{pol} refers to the induced amount of charges due to the spontaneous polarization and the piezoelectric polarization. σ_{pol} can be expressed as following formula [11].

$$\sigma_{pol} = \mathrm{P(AlGaN)} - \mathrm{P(GaN)} = \mathrm{P_{SP}(AlGaN)} + \mathrm{P_{PE}(AlGaN)} - \mathrm{P_{SP}(GaN)},$$

$$\mathrm{P_{PE}(x)} = 2\frac{a(x) - a(0)}{a(0)}\left[e_{31}(x) - e_{33}(x)\frac{C_{13}(x)}{C_{33}(x)}\right]$$

$a(x)$, $C_{ab}(x)$, and $e_{ab}(x)$ refer to AlGaN lattice constant depending on Al mole fraction, polarization constant depending on Al mole fraction, and coefficient of elasticity depending on Al mole fraction, respectively. Recent reported critical thickness of AlGaN layer which may differ by the epitaxial growth technique is from 5 to 10 nm [32].

Generally, AlGaN/GaN HEMT's gate-recessed structure is fabricated by dry etching technique which employs induced coupled plasma (ICP) etcher. However, this technique may bring about etching damage on the device surface due to reactive ions accelerated by the bias. This physical damage affects epitaxial layer of AlGaN/GaN HEMT negatively and also may induce surface states. Eventually, the electrical characteristics of the device may be degraded.

In order to avoid etching damage due to the plasma, several wet etching techniques also have been proposed so far. Wet etching technique has been widely investigated because of its simplicity and free of plasma damage. The most widely employed aqueous solution for GaN wet etching is Potassium hydroxide (KOH) solution. However, it is widely known that the Ga-face GaN has a difficulty in etching by KOH solution [33]. This can be a serious issue since most AlGaN/GaN HEMTs employs Ga-face AlGaN and GaN as its epitaxial layer. Many additional treatments during KOH wet etching have been reported such as exposing UV light [34, 35], applying bias [36], or using potassium persulphate ($K_2S_2O_8$) [37]. In this thesis, I

also employed KOH solution for the wet etching and interesting results are investigated. The detail results are introduced in chapter 4.

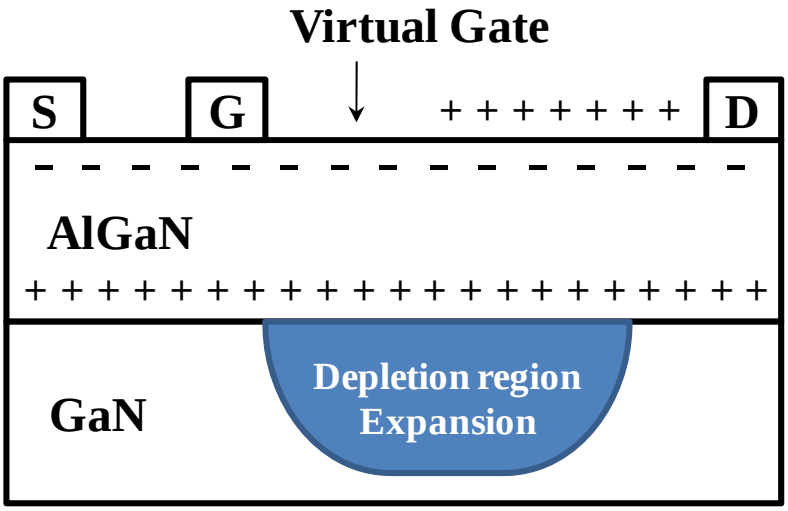

Figure 2-4: Formation of Virtual Gate by electrons' trapping

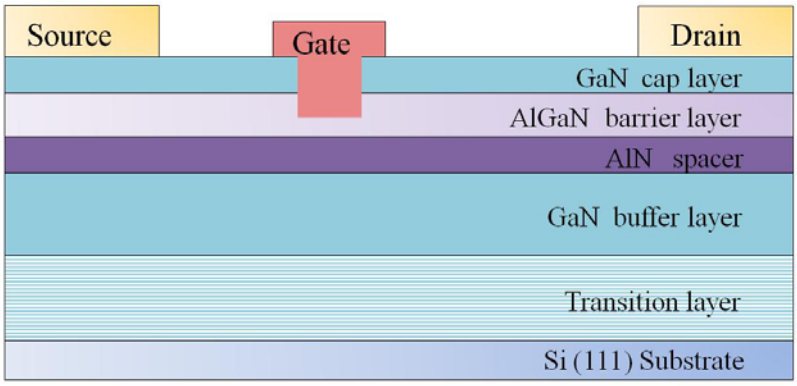

Figure 2-5: Example of gate-recessed normally-off AlGaN/GaN HEMT

2.3. Recent Research of RF-sputtered HfO_2 for the Gate Insulator

To resolve two issues I mentioned in previous sections, my senior colleague and I studied deep into a RF-sputtered HfO_2 for metal-oxide-semiconductor (MOS) structure [38]. Since MOS structure effectively blocks and suppresses the surface leakage current during both off-state and on-state, my laboratory could fabricate high-performance normally-off AlGaN/GaN MOS HEMTs by employing RF-sputtered HfO_2 as a gate insulator. The specific results of the device is exhibited in chapter 4. In this section, the material characteristics of HfO_2 for AlGaN/GaN HEMTs deposited by RF-sputtering method will be introduced. Also, various electrical characteristics of AlGaN/GaN MOS HEMTs employed HfO_2 is shown in order to demonstrate the superiority of RF-sputtered HfO_2. The cross-sectional view of fabricated AlGan/GaN MOS HEMT employing RF-sputtered HfO_2 is shown in Fig. 2-6.

2.3.1. Sputtering Condition Optimization and Weak Crystallizability of RF-Sputtered HfO_2

To employ RF-sputtered HfO_2 to AlGaN/GaN HEMTs, the deposition condition had to be optimized. The most important condition was sputtering power. In order to figure out the relationship between sputtering power and device performance, the drain leakage current of RF-sputtered HfO_2 employed AlGaN/GaN HEMTs were measured. Figure 2-7 shows the relationship between sputtering power and the leakage

current of the device. As shown in Fig. 2-7, in order to employ RF-sputtered HfO_2 to the device, sputtering power has to be low as much as possible. This result coincides with one report that high sputtering power wreaks damage to the surface of the sample.

Also, to investigate the insulator quality, X-ray Diffraction (XRD) and auger electron spectroscopy (AES) is measured for deposited RF-sputtered HfO_2 as shown in the Fig. 2-8. As shown in the XRD result, RF-sputtered HfO_2 shows weak peaks of the (2 0 0) and (2 2 0) tetragonal phases at around 35^0 which demonstrate weak crystallizability. In addition, AES result shows that the 1:1.8 Hf and Oxygen proportion which quiet matches well with the origin atomic proportion 1:2.

2.3.2. Transfer and Dielectric Breakdown Properties

Figure 2-9 shows the transfer characteristic of fabricated device when the V_{DS} is 5 V. The on/off current ratio is measured at $I_{D,ON}$ when V_{GS}= 0 V and $I_{D,OFF}$ when V_{GS}= −10 V. The measured on/off current ratio was over than 11 orders which is considerably high enough. High on/off current ratio indicates HfO_2 is successfully blocking gate leakage current and isolation leakage current between source and drain as well. Moreover, because of the high-*k* characteristic of HfO_2, the V_{TH} of the device did not shift much to the negative direction.

Also, to figure out the possibility of the normally-off device application, dielectric breakdown characteristic of 15 nm thickness of RF-sputtered HfO_2 was investigated as shown in Fig. 2-10. As you can see in the graph, RF-sputtered HfO_2 successfully sustains up to positive gate bias of 10 V.

This result demonstrates that HfO_2 is also applicable to normally-off AlGaN/GaN MOS HEMT even deposited by sputtering method.

2.3.3. DC and Pulsed *I-V* Characteristics

In order to investigate the surface passivation effect, I also measured DC and pulsed output *I-V* characteristic of the HEMT and the MOS-HEMT with RF-sputtered HfO_2 as shown in Fig. 2-11. As shown in two graphs, under the same pulsed bias condition, the drain current degradation of the MOS-HEMT is less than that of conventional HEMT. This result verifies that the RF-sputtered HfO_2 successfully suppresses surface trap effects so that it may be a good material for AlGaN/GaN MOS-HEMT's current collapse prevention.

2.3.4. Capacitance-Voltage Characteristics

Figure 2-12 (a) shows capacitance-voltage (*C-V*) characteristics of AlGaN/GaN MOS-HEMTs with RF-sputtered HfO_2. In order to investigate response of electrons to HfO_2/GaN interface, maximum V_{GS} was varied with fixed frequency of 1 MHz. In the case of −10 to −0.5 V sweeping range, a small hysteresis of 100 mV near V_{TH} was investigated. However, in the case of −10 to 5 V sweeping range, a large hysteresis of 1.1 V was investigated. This result indicates the existence of acceptor-like traps at the interface between HfO_2 and GaN surface.

Also, Fig. 2-12 (b) shows the C-V characteristics with various measuring frequency of 1, 10, 100 kHz, and 1 MHz. At negative gate bias with all frequency, identical hysteresis was observed. On the contrary, in the case of positive gate bias, lower frequency causes higher capacitance value and the larger hysteresis. This result also indicates electron trapping at the interface between HfO_2 and GaN surface is a slow process by seeing that the response to the frequency lower than 1 MHz.

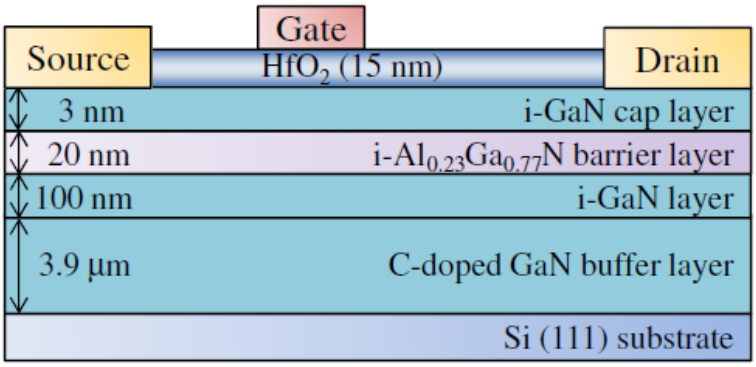

Figure 2-6: Cross-sectional view of the proposed AlGaN/GaN MOS-HEMT with HfO_2 [38]

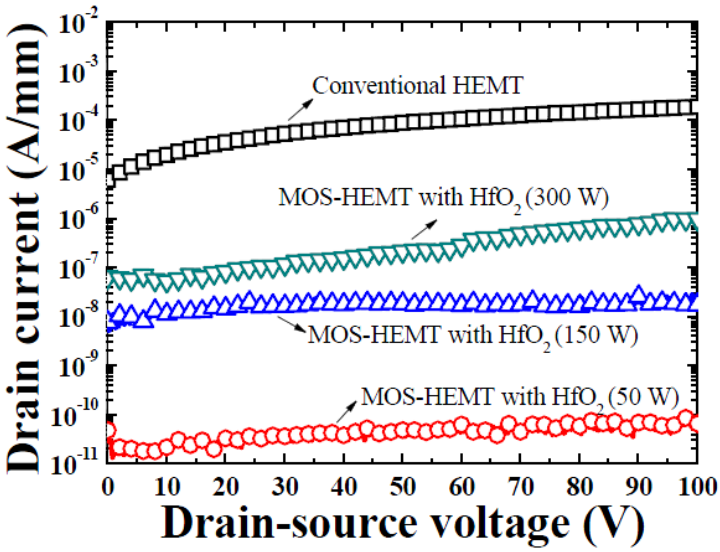

Figure 2-7: Drain leakage current of AlGaN/GaN HEMT and MOS-HEMTs with HfO_2 sputtered at various power [38]

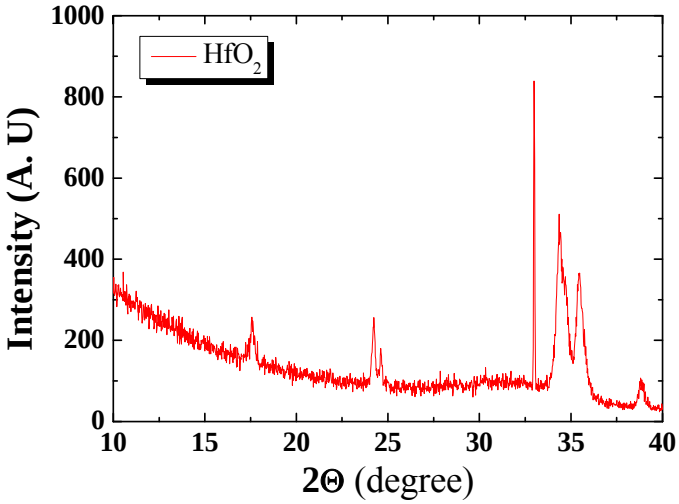

(a)

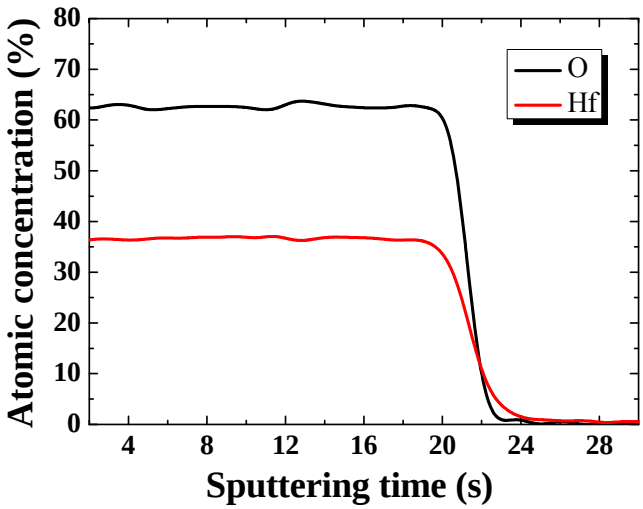

(b)

Figure 2-8: (a) XRD spectra of the RF-sputtered HfO_2 **(b)** AES-depth profile HfO_2/Si substrate [38]

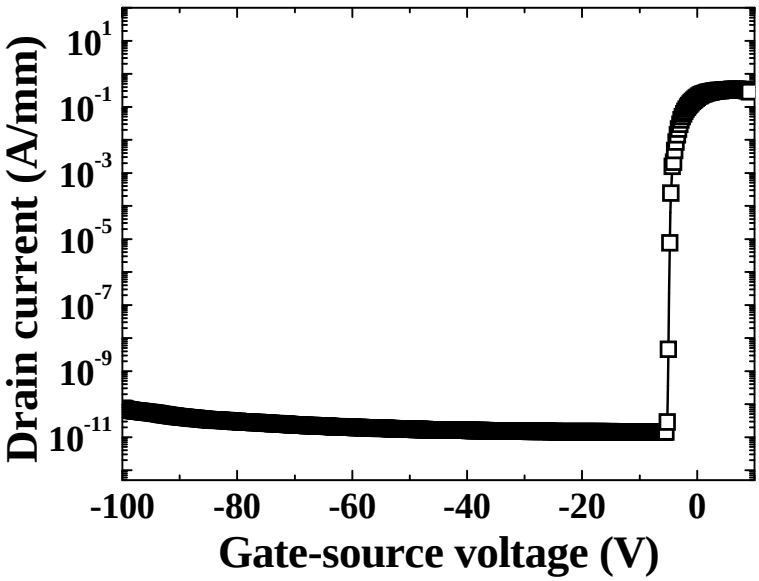

Figure 2-9: Transfer characteristic of AlGaN/GaN MOS-HEMT with HfO_2 [38]

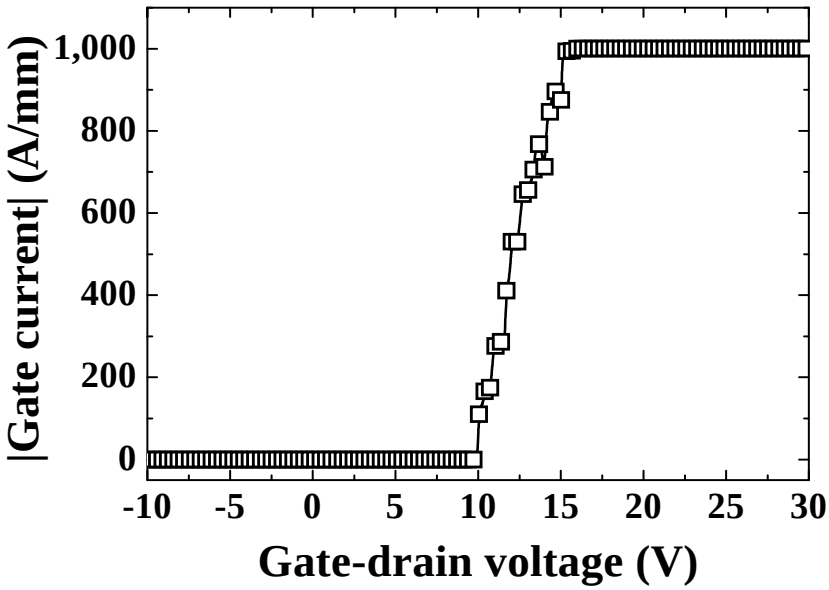

Figure 2-10: Forward breakdown voltage of the gate-drain diode of MOS-HEMT with RF-sputtered HfO_2 [38]

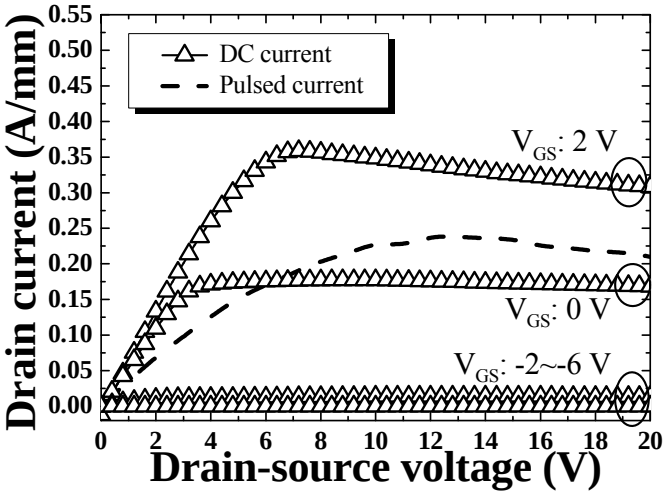

(a)

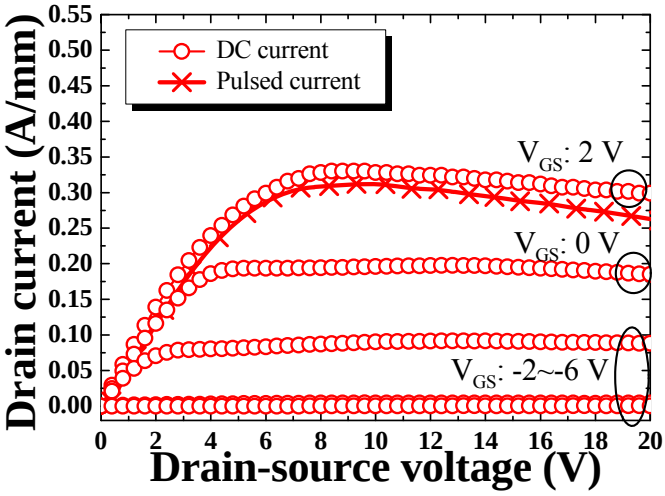

(b)

Figure 2-11: DC and pulsed *I-V* characteristics of **(a)** the conventional HEMT and **(b)** AlGaN/GaN MOS-HEMT with HfO_2 [38]

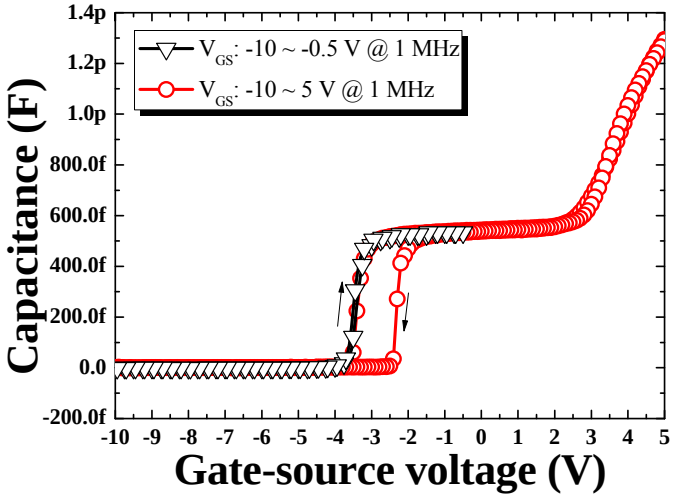

(a)

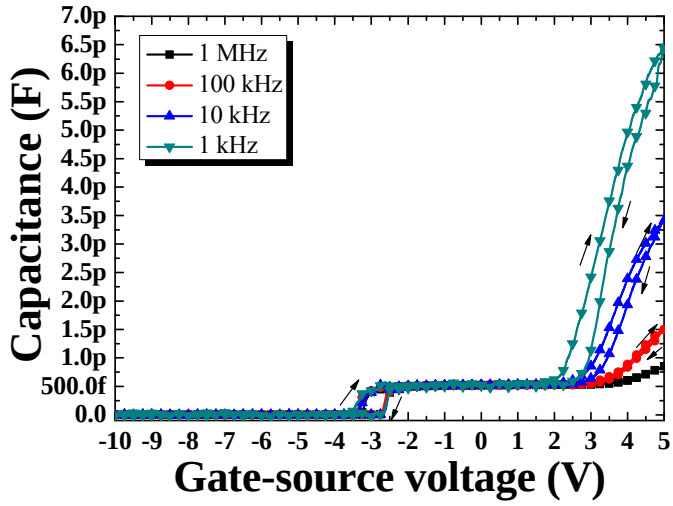

(b)

Figure 2-12: (a) *C-V* characteristics of AlGaN/GaN MOS-HEMTs **(b)** *C-V* characteristics with various measuring frequency [38]

2.4. Summary

AlGaN/GaN HEMTs have attracted an attention for next-generation power devices due to wide bandgap properties such as a high critical electric field and a low intrinsic carrier concentration. Due to highly conductive two-dimensional electron gas (2DEG) induced by the discontinuity of conduction band and piezoelectric polarization, low on-resistance and fast switching speed are AlGaN/GaN HEMT's strong merits.

However, the surface state issue and the normally-on characteristic are two major issues of AlGaN/GaN HEMTs. Electrons trapping at surface states degrade the transconductance and the forward characteristics. Also, the large leakage current due to surface states will decrease the breakdown voltage of AlGaN/GaN HEMTs. In addition, due to the innate characteristic of the 2DEG inducement in AlGaN/GaN HEMT, normally-on characteristic is another important issue and this must be solved for AlGaN/GaN HEMTs commercialization.

To solve two issues above, MOS-HEMT with RF-sputtered HfO_2 was proposed and investigated. The device showed good blocking characteristics due to the passivation effect of HfO_2. Also, weak crystallizability of RF-sputtered HfO_2 was investigated by XRD and AES measurement. These results indicates that RF-sputtered HfO_2 is may be a suitable gate insulator for the fabrication of normally-off AlGaN/GaN MOS-HEMTs.

Chapter 3

3. AlGaN/GaN HEMTs Employing H_2O Annealing

3.1. Overview

The soft breakdown characteristic of AlGaN/GaN HEMTs caused by surface leakage current is a critical issue as introduced in section 2.2.1 [39]. Earlier, one of my coworkers reported a very low leakage current and a high breakdown voltage of 1140 V of AlGaN/GaN HEMTs employing O_2 annealing [40]. The electrons from the gate trapped into Ga vacancies in the thermally oxidized GaO_X layer suppress the surface leakage current. However, H_2O annealing induces a more active reaction between Ga and O due to H_2O's higher permeation probability, smaller molecular size compared to O_2 and its lower activation energy. The molecule diameter of H_2O is smaller than that of O_2 and H_2O exhibits greater solubility than that of O_2 in a solid material. Thus, the permeation probability of H_2O is

considerably higher than that of O_2 [41]. The diameter of the H_2O molecule is 0.28 nm while the diameter of the O_2 molecule is 0.36 nm. The activation energy of H_2O for oxidation is lower than that of O_2 for oxidation. The activation energy of H_2O for oxidation in GaN is 210 ± 10 kJ/mol, whereas that for O_2 is 300 kJ/mol [42]. Thus, H_2O permeates into AlGaN/GaN more than O_2 and increases the number of reactions between O and Ga.

In this chapter, I propose efficient GaO_x formation by H_2O annealing on the surface of AlGaN/GaN HEMTs of which reverse blocking characteristics was improved. H_2O annealing on AlGaN/GaN HEMTs has scarcely reported. The unintentionally formed Ga vacancies of the GaO_x on GaN cap layer may be regarded as deep traps [43]. Deep traps on the surface of the device represented the main mechanism of the increase in the breakdown voltage of AlGaN/GaN HEMTs [44].

In section 3.3, I compared GaO_x growth results by investigating the results of X-ray photoelectron spectroscopy (XPS) and Auger electron spectroscopy (AES). In section 3.4, I also measured various electrical characteristics such as the DC and pulsed output characteristics of the device in order to investigate the reverse blocking characteristics of AlGaN/GaN HEMTs.

3.2. Device Fabrication and Structure

The fabricated AlGaN/GaN HEMTs are fabricated by four main processes such as mesa etching, Ohmic contact formation, H_2O annealing, and Schottky contact formation as shown in Fig. 3-1. The systematic structure of the fabricated AlGaN/GaN HEMTs employed H_2O annealing is shown in the last image of Fig. 3-1.

AlGaN/GaN heterostructure was grown on a Si(111) substrate. The structure grown by metal-organic chemical vapor deposition comprises the following specific layers: the nucleation layer, a 3.9-μm-thick C-doped GaN buffer layer, a 100-nm-thick unintentionally-doped (UID) GaN layer, a 20-nm-thick UID-$Al_{0.23}Ga_{0.77}N$ barrier layer, and a 3-nm-thick UID-GaN cap layer. The Hall measurement of the conventional sample yielded 4.34×10^{12} cm^{-2} and 1860 $cm^2/(V\cdot s)$ at the room temperature.

Mesa isolation using Cl_2 and BCl_3-based inductively coupled plasma (ICP) etching was performed in order to define the active region. The 300 nm-deep mesa structures were formed by ICP etcher.

Then, ohmic metal of Ti/Al/Ni/Au (20/80/20/100 nm) for the source and drain was formed by an e-gun evaporation and a lift-off process. After the deposition of the layer of ohmic metal, the annealing was done at 880 ^{o}C for 40 s under an N_2 ambient for ohmic alloy. The ohmic contact resistance was measured to be 0.58 Ω·mm by using transfer length method (TLM).

Prior to the annealing process, the acetone and methanol cleaning process were done for 300 s each, after 30:1 buffered oxide etchant cleaning was done for 30 s in order to remove a native oxide of GaN. After

cleaning the devices, I applied O_2 annealing and H_2O annealing to each device in a rapid thermal annealing chamber for 300 s at 500 ^{o}C. I used N_2 as a carrier gas for the H_2O annealing at a flow rate of 2 slm.

Finally, I formed a Schottky contact of Ni/Au/Ni (30/150/30 nm) for the gate electrode. No annealing process was conducted to the Schottky gate. The gate length, gate-drain distance, and gate width were 3, 20, and 50 μm, respectively.

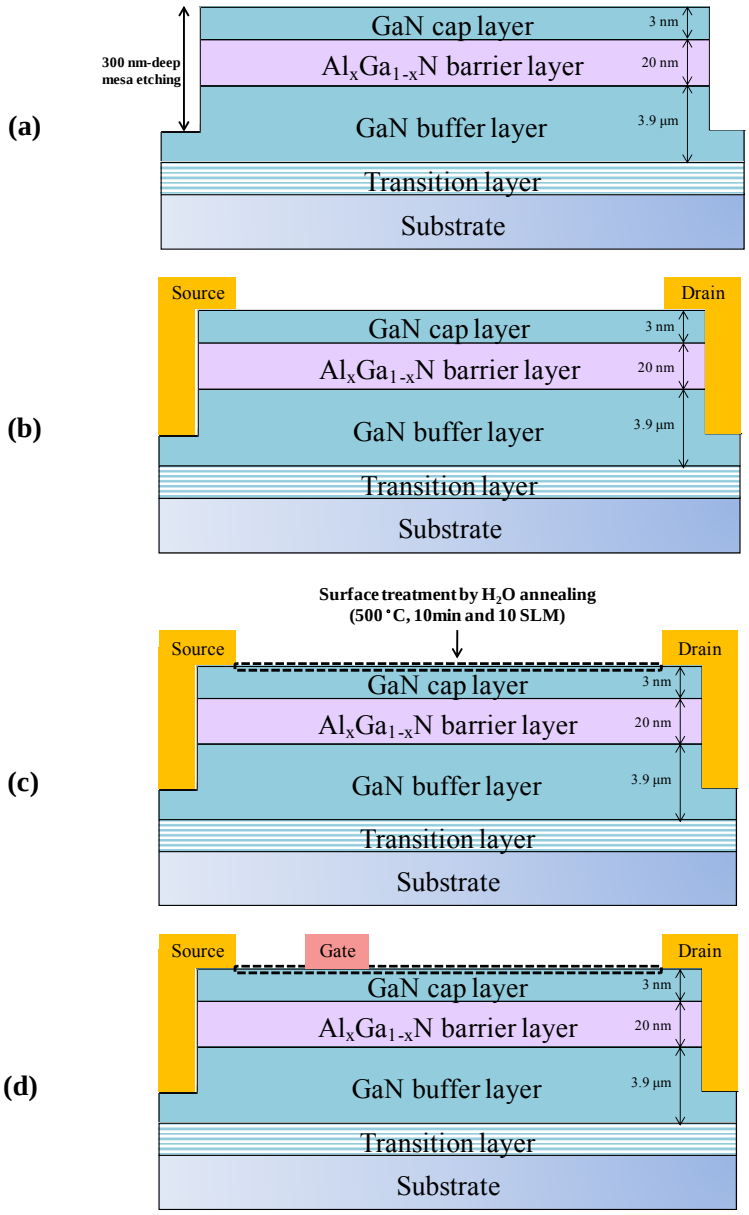

Figure 3-1: Fabrication process; **(a)** mesa etch, **(b)** Ohmic contact, **(C)** H_2O annealing and **(d)** Schottky contact

3.3. Comparison of GaO_X Material Properties formed by H_2O and O_2 Annealing

In this section, I will investigate the material properties of GaO_X on GaN cap layer to compare how GaO_X is efficiently formed by each O_2 annealing and H_2O annealing method. In order to analyze the elemental composition of the surface of the device, I investigated the annealed samples by XPS. Also, in order to analyze the chemical composition, not only solid surface but also several nano-meters depth from the surface, I employed AES for the investigation as well.

3.3.1. XPS Investigation Result

A XPS photograph of the chemical analysis profiles showing the surface oxide above the GaN cap layer is shown in the Fig. 3-2. The XPS analysis was performed by an AXIS-HSi XPS instrument. The shift in the electro-binding-energy peaks of O 1s after the H_2O annealing of the GaN cap layer was exhibited. The electron binding energy of O 1s was observed to shift from 531.75 to 532.35 eV in the case of H_2O annealing and 531.75 to 532.15 eV in the case of O_2 annealing. This indicated that surface oxidation by H_2O annealing induced a greater reaction than O_2 annealing between O and Ga which resulted in GaO_X on the surface. In addition, the area percentage related to the GaO_X was 16.1% when AlGaN/GaN specimen was annealed in H_2O ambient. However, for the specimen annealed in O_2 ambient, it was 12.8 % while the specimen without annealing only showed an area percentage of 10.5 %.

3.3.2. AES Investigation Result

The Auger Electron Spectroscopy (AES) is a method that investigating the elemental distribution of the sample's surface. The mechanism of AES is exposing electron beam to the sample and analyzing energy spectrum of Auger electron which is from atoms in the sample.

The AES-depth profile from surface to AlGaN/GaN to investigate the oxygen's permeation probability during annealing processes is shown in Fig. 3-3. The AES was performed using a PHI 660 Auger microprobe. The oxygen atomic concentration gradually decreased with the sputtering time. However, the oxygen concentration of the H_2O annealed specimen distinctively exhibited a higher value than that annealed with O_2. The H_2O annealing exhibited the higher permeation probability of oxygen on the surface than the O_2 annealing.

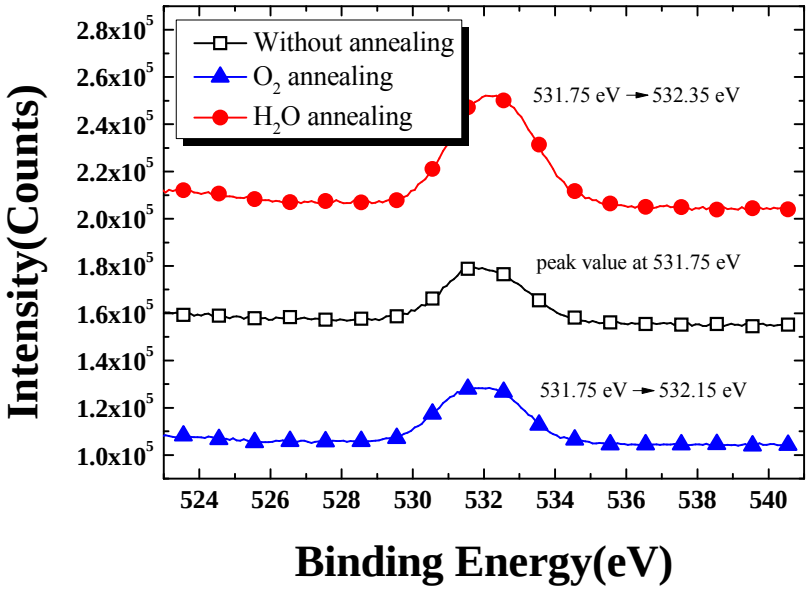

Figure 3-2: XPS analysis of the conventional and annealed specimen

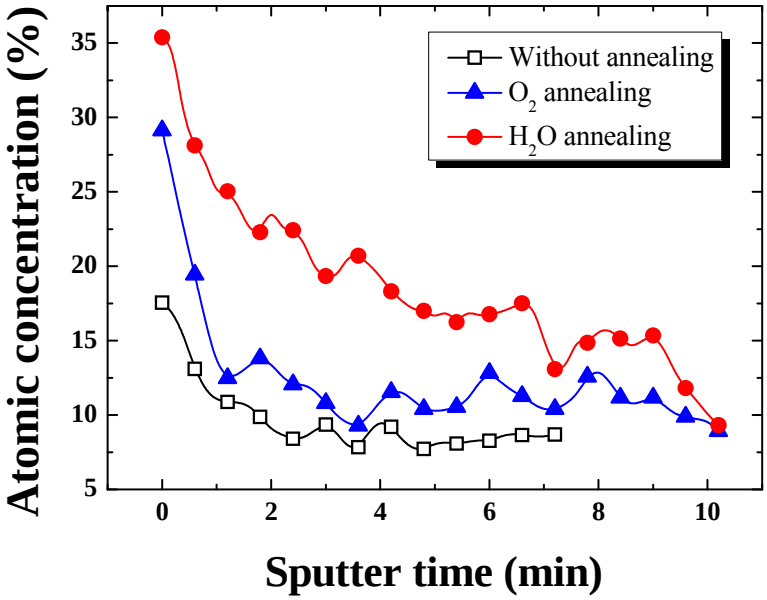

Figure 3-3: AES analysis of the conventional and the annealed specimen

3.4. Electrical Properties of AlGaN/GaN HEMTs Employing H_2O Annealing

The electrical characteristic of AlGaN/GaN HEMTs employing H_2O annealing and O_2 annealing and the conventional devices are measured. AlGaN/GaN HEMTs were not packaged and measured in the probe station. The DC characteristics such as output characteristic, leakage current, and breakdown voltage are measured by using B1500A and 370A curve tracer. The pulsed *I-V* of AlGaN/GaN HEMT is also measured in order to compare trap state between H_2O annealed, O_2 annealed and conventional devices. The pulsed *I-V* of AlGaN/GaN HEMT is measured in the probe station by using B1500A. The pulse signal was applied to both drain and gate at the same time. At last, I investigated considerable enhanced DC characteristics by H_2O annealing, however, pulsed *I-V* characteristic was somewhat degraded due to deep traps existence at the surface of the device.

3.4.1. Drain Leakage Current Characteristics

Figure 3-4 shows the drain leakage current of AlGaN/GaN HEMTs according to three different annealing conditions at V_{GS} of –10 V. AlGaN/GaN HEMT employing the annealing process before the formation of the Schottky contact decreased considerably the leakage current of about 10^4 times. The conventional AlGaN/GaN HEMT had the drain leakage current of 666.0 μA/mm. However, the drain leakage current of the device with O_2 annealing was 60.1 nA/mm while that of the device with H_2O annealing was only 13.1 nA/mm.

The high leakage current of the conventional device is mainly induced by shallow traps on the surface, which are generated by surface damages during the process and dislocation. However, the drain leakage currents of the device with H_2O or O_2 annealing are considerably decreased. The formation of GaO_X by the annealing process exhibits an amorphous phase comprising various bonding and non-bonding states, such as Ga and O vacancies. In the reverse blocking mode in AlGaN/GaN HEMTs at $V_{GS} < V_{TH}$, the gate edge of the drain side exhibits a high electric-field such that hot electrons are injected from the gate into the GaO_X film on the GaN cap layer. The injected electrons into the deep traps such as Ga vacancies have a low probability of de-trapping so that the depletion region between the gate and drain is extended and the leakage current is suppressed. Furthermore, I can expect more efficient suppression by H_2O annealing than by O_2 annealing because the drain leakage current level is four times smaller.

3.4.2. Breakdown Voltage Characteristics

Figure 3-5 shows the breakdown voltage of the three different AlGaN/GaN HEMTs. The breakdown voltage was defined as at the leakage current of 1 mA/mm. The breakdown voltage of the conventional device was 598 V while this of the device with O_2 annealing was 1512 V due to the formation of GaO_X on the surface. Moreover, the device which underwent H_2O annealing shows the highest breakdown voltage of 1674 V.

The conventional device shows soft breakdown and exhibits a large

leakage current in proportion to the reverse voltage. However, The O_2 and H_2O annealed devices exhibits hard breakdown and also low level of the leakage current until breakdown. By these results of the breakdown voltage, I verified the passivation effect of H_2O annealing. My experimental results indicate that H_2O annealing induces more combinations between Ga and O than O_2 annealing, which prevents electron trapping on the surface of AlGaN/GaN.

3.4.3. DC Output Current Characteristics

A high-temperature process may cause thermal damages to AlGaN/GaN HEMTs. Thus, I measured the DC output characteristics of AlGaN/GaN HEMTs as shown in the Fig. 3-6. The drain current was measured while sweeping the gate voltage from −2 to 2 V in 2 V steps. The drain current was not changed considerably by the O_2 annealing. However, the drain current of the device annealed with H_2O was reduced and the value of the on-resistance was increased.

I measured the ohmic contact resistance in an effort to specify ohmic contact using transmission line measurement. The ohmic contact resistance in the case of O_2 annealing was 0.60 Ω·mm while this of H_2O annealing was 0.67 Ω·mm. Considering this marginal difference of the contact resistances, I speculate that the main reason for degrading the on-resistance and DC on-current is the deep traps in the GaO_X layer on the surface. It was suggested that the deep traps are responsible for the current collapse and the increase in the on-resistance in AlGaAs/GaAs HEMTs [44, 45].

3.4.4. Pulsed *I-V* Characteristics

AlGaN/GaN HEMTs have surface state issue that may cause gate dispersion problem in the case of switching operation so that on-resistance may increase. This problem can be investigated by applying pulse signal at the gate electrode or drain electrode. Pulsed *I-V* measurement induces electrons trapping at the surface trap and changes the bias to forward direction abruptly. By measuring drain current when the bias is forward direction, the reduced current due to trapping can be measured. In the case of the shallow trapping, I can investigate traps by short pulse duration since the time gap between trapping and detrapping is short. On the other hand, in the case of the deep trapping, I should increase pulse duration in order to investigate the existence of deep traps. It is widely known that the activation energy of shallow traps at the surface of conventional device is about 38 meV so that 500 ns of pulse duration is demanding to measure. Also, the activation energy of deep traps is known to be at least 0.31 eV so that about 21.6 μs to measure.

I measured the pulsed *I-V* current in order to investigate the amounts of deep traps in the GaO_X layer on AlGaN/GaN HEMT. The gate pulse was swept from –6 to 2 V (pulse width/period= 5 μs/1 ms) and drain pulse was also applied at the same time as shown in Fig. 3-7. Gate voltage was varied as 2 V, 0 V and –2 V for the comparison purpose. Also, drain pulse was applied from 0 V to applied bias which is from 1 V to 20 V. Applied bias increased 1 V as one period ends and drain current was measured when the pulse is applied.

The result of the pulsed *I-V* current when the gate voltage is 2 V, 0 V, and –2 V is exhibited in Fig. 3-8. It has been well known that O_2-related

treatment generates deep traps and degraded pulsed *I-V* [45, 46]. As shown in Figure 3-8, the O_2-annealed device exhibits a reduced pulsed on-current indicating the existence of deep traps. Additionally, I performed the H_2O and O_2 annealing to form GaO_X under Schottky contact to improve the Schottky barrier height and gate leakage current before the gate formation [45]. These results show that the device annealed with H_2O exhibits a longer emission time than that of the device annealed with O_2 and without any annealing process due to the increased number of deep traps in the GaO_X on the surface.

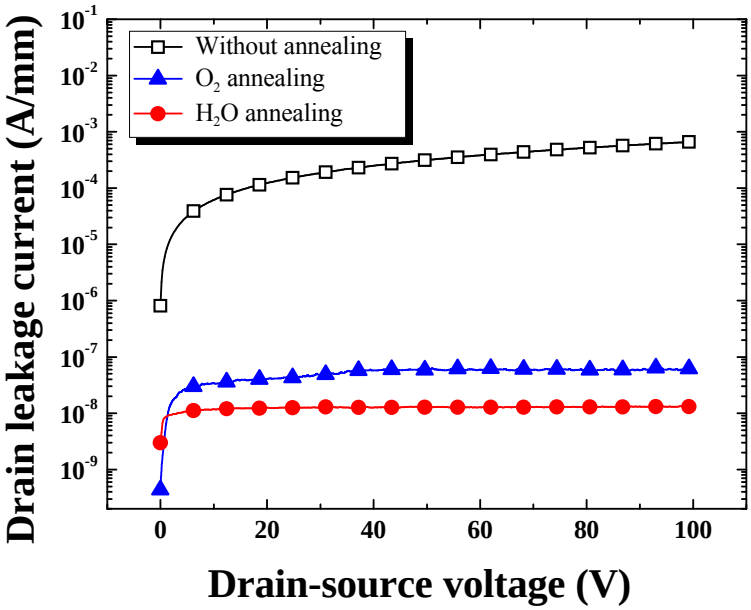

Figure 3-4: Measured drain leakage current of the conventional and annealed devices

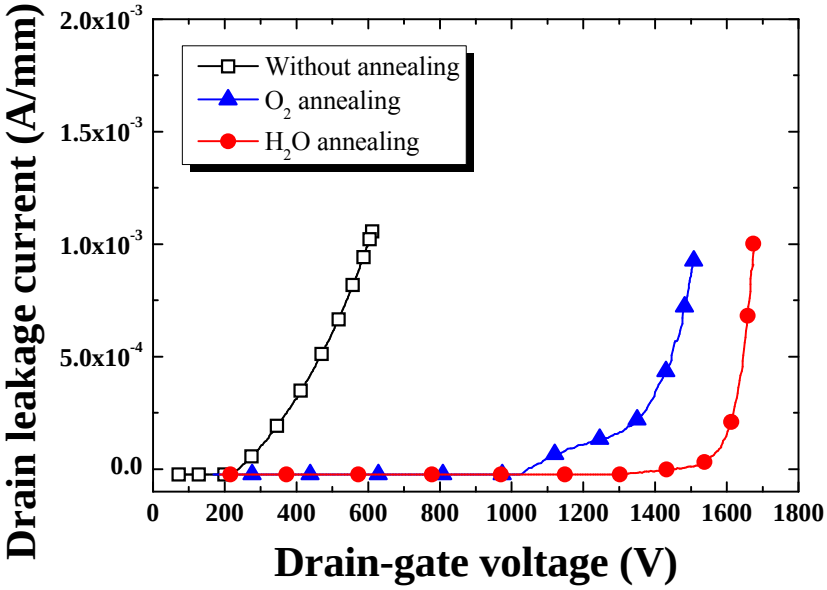

Figure 3-5: Breakdown voltage of the conventional and annealed devices

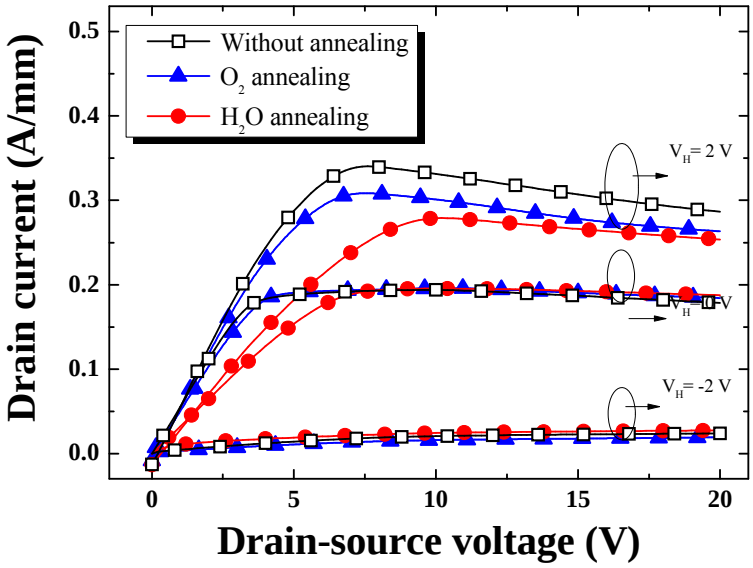

Figure 3-6: DC output current of the conventional and annealed devices

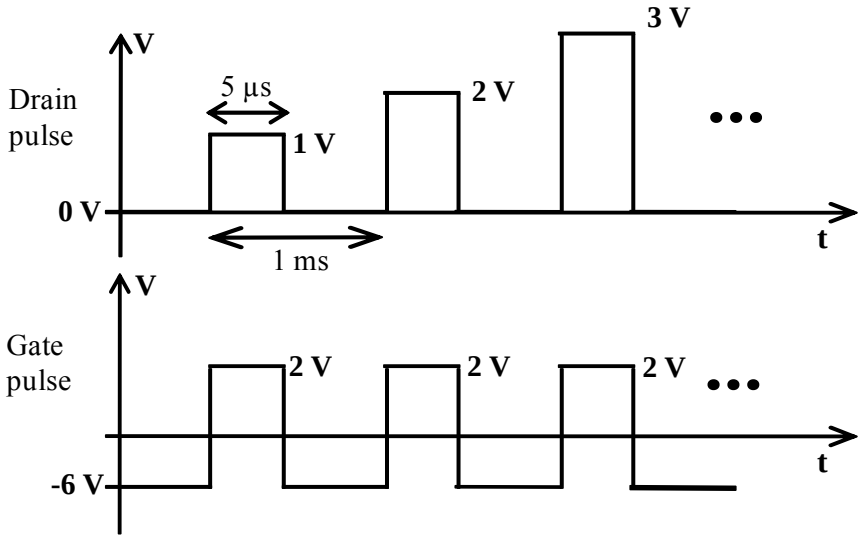

Figure 3-7: Applied gate and drain bias of pulsed *I-V*

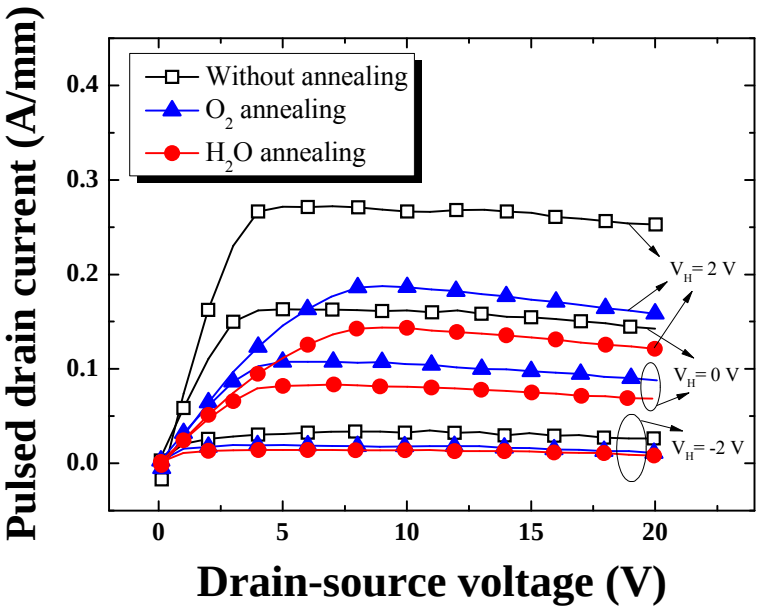

Figure 3-8: Pulsed *I-V* characteristic of the conventional and annealed devices

3.5. Summary

I have successfully fabricated AlGaN/GaN HEMTs by means of simple H_2O annealing. I compared H_2O annealing to O_2 one and investigated the characteristics of the breakdown voltage and the leakage current in AlGaN/GaN HEMTs. The breakdown voltage and drain leakage current of AlGaN/GaN HEMT employing the H_2O annealing treatment were 1674 V and 13.1 nA/mm, while those values with the O_2 treatment were 1512 V and 60.1 nA/mm. The conventional HEMT without annealing exhibited the breakdown voltage of 598 V and the drain leakage current of 666.0 μA/mm. The H_2O annealing formed successfully GaO_X on the surface of AlGaN/GaN. My experimental results show efficient suppression of shallow traps and existence of deep traps on the surface of the device. However, deep traps in GaO_X on the surface of the device degraded pulsed *I-V* characteristic of the devices. Thus, more research will be needed in the case of RF application. However, in the case of DC application, H_2O annealing may be a promising method to fabricate high-performance AlGaN/GaN HEMTs.

Chapter 4

4. Normally-off AlGaN/GaN Metal-Oxide-Semiconductor HEMTs

4.1. Overview

Previously reported AlGaN/GaN HEMTs have a normally-on characteristic with threshold voltage (V_{TH}) of –3 to –6 V due to the polarization-induced 2DEG as introduced in section 2.2. In order to control the threshold voltage of the device, I adopted electrode-less wet etching technique using KOH-based solution. So far, the simple wet etching employing only KOH has been reported scarcely.

Also, without high-quality gate insulator, we cannot fabricate the normally-off device because of the limited V_{GS} swing range. If positive voltage is applied to the gate electrode, which is higher than that of source electrode, the Schottky barrier of gate electrode will be lowered so that the

considerable gate leakage current will deteriorate the electrical characteristic of the device. In order to fabricate the device with a low level-leakage current under both a positive and a negative bias, a metal-oxide-semiconductor (MOS) structure maybe desirable for the high voltage and high on/off current ratio AlGaN/GaN HEMTs.

Various gate insulator materials such as Si_3N_4 [21], SiO_2 [22] have been reported. A very thin layer of SiO_2 or Si_3N_4 is essential for the normally-off AlGaN/GaN HEMTs because of their low-k characteristics. However, a very thin gate insulator is not applicable since it may induce hot carrier-induced gate leakage current and it results in a narrow V_{GS} swing range. Therefore, high-*k* gate insulator materials such as HfO_2 [47, 48] and ZrO_2 [49] are desirable. Because they suppress the negative shift of the threshold voltage and prevent a device failure due to dielectric breakdown during the reverse blocking operation.

In this chapter, I will report the normally-off recessed structure AlGaN/GaN MOS-HEMTs by simple KOH wet etch. I successfully fabricated the normally-off AlGaN/GaN HEMTs with high breakdown voltage exceeding 1500 V. In chapter 4.3., I describe about the KOH wet etching results. The recessed depth was well controlled by KOH-wet etching time. Also, the smooth surface was achieved by this method. In chapter 4.4., I show various electrical characteristics AlGaN/GaN MOS HEMTs employing simple KOH wet etching and RF-sputtered HfO_2 introduced in the section 2.3.

4.2. Device Fabrication and Structure

The process of the fabricated AlGaN/GaN HEMTs is shown in Fig. 4-1. AlGaN/GaN heterostructure was grown on a Si(111) substrate. The structure grown by metal-organic chemical vapor deposition comprises the following specific layers: the nucleation layer, a 3.9-μm-thick C-doped GaN buffer layer, a 100-nm-thick unintentionally-doped (UID) GaN layer, a 20-nm-thick UID-$Al_{0.23}Ga_{0.77}N$ barrier layer, and a 3-nm-thick UID-GaN cap layer on AlN nucleation layer. Mesa isolation using Cl_2 and BCl_3-based inductively coupled plasma etching was performed in order to define the active region and the etched depth was about 300 nm-deep.

After mesa isolation, I deposited SiO_2 by plasma enhanced chemical vapor deposition (PECVD) for the wet etching mask. The thickness of SiO_2 was 200 nm and I etched SiO_2 at the gate region of the sample by RIE etcher. After that, I dipped samples into 1 M/L (Mol/Liter) KOH solution for 50, 100, 150, and 200 s, respectively and the temperature was room temperature. Ti/Al/Ni/Au (20/80/20/100 nm) was used for the source and the drain. Ohmic metals were formed by e-gun evaporation and a lift-off process. Prior to HfO_2 sputtering, I dipped the sample into 30:1 buffered oxide etchant for 30 s.

The 15 nm-thick HfO_2 was deposited by RF-sputtering power of 50 W. The pressure, temperature, time and the gas flow were 3 mTorr, room temperature, 1200 s and Ar of 15 sccm, respectively. Finally, Schottky contact, Ni/Au (30/150 nm), was formed on RF-sputtered HfO_2 insulator by e-gun evaporator. Lastly, I eliminated the HfO_2 gate insulator on the source and the drain electrode for the measurement. The gate length, the gate-drain distance, and the width were 3, 20, and 50 μm, respectively.

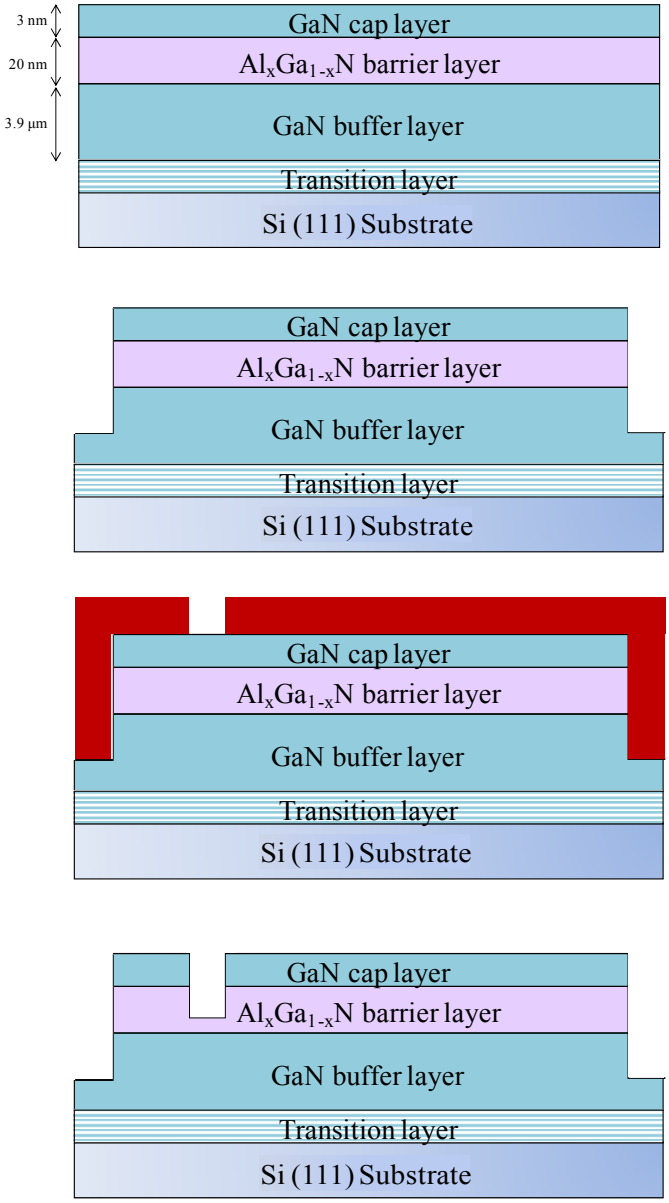
3 nm
20 nm
3.9 µm
GaN cap layer
$Al_xGa_{1-x}N$ barrier layer
GaN buffer layer
Transition layer
Si (111) Substrate
GaN cap layer
$Al_xGa_{1-x}N$ barrier layer
GaN buffer layer
Transition layer
Si (111) Substrate
GaN cap layer
$Al_xGa_{1-x}N$ barrier layer
GaN buffer layer
Transition layer
Si (111) Substrate
GaN cap layer
$Al_xGa_{1-x}N$ barrier layer
GaN buffer layer
Transition layer
Si (111) Substrate

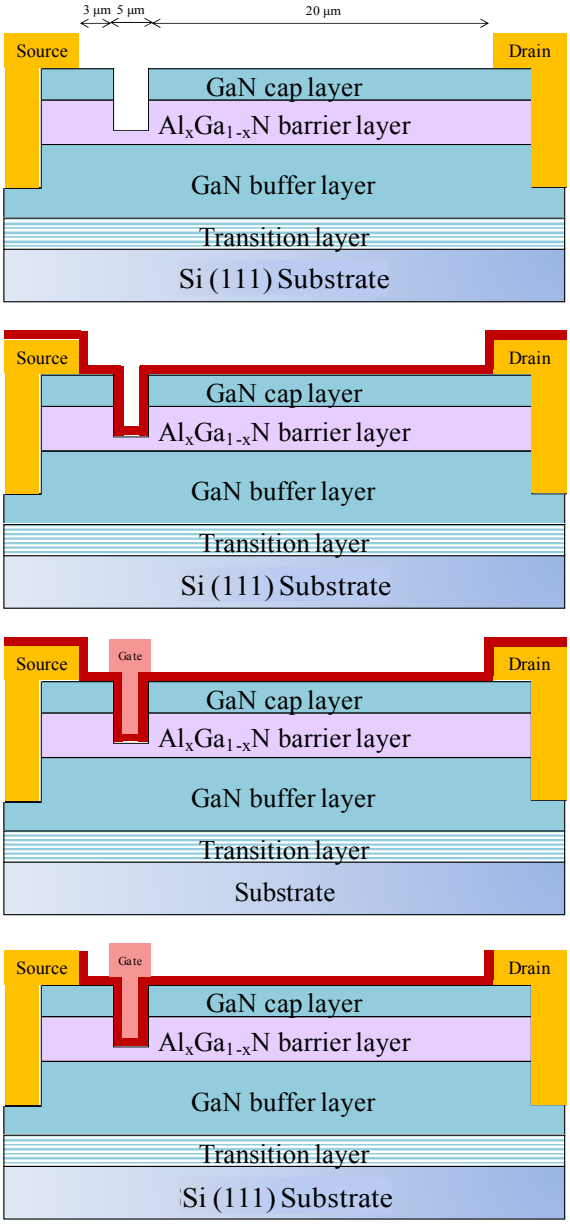

Figure 4-1: The fabrication flow and the cross-sectional view of proposed gate-recessed AlGaN/GaN MOS HEMTs

4.3. The results of KOH wet etching

In order to fabricate normally-off AlGaN/GaN HEMTs, the recessed-gate structure has been considered as advantageous for its simplicity and high transconductance due to reduced distance between the gate electrode and 2DEG channel. Various methods have been suggested and among those methods, wet etching technique has been dealt as a better approach than dry etching because it is free from etching damage.

Many GaN wet etching technique have been proposed including photo-assisted cryogenic etch (PAC) [18], photo-assisted anodic etch, photo enhanced electrochemical (PEC) wet etch, and PEC binary etch using $K_2S_2O_8$ and KOH.

In this thesis, I successfully etched GaN by KOH aqueous solution only with good controllability, reliability and uniformity. The etched depth was measured by Atomic Force Microscopy (AFM) measurement. Also by comparing the threshold voltage of all fabricated devices, I investigated the uniformity of simple KOH wet etching.

4.3.1. AFM measurement results

AFM is one type of microscope that can measure the sample's surface characteristic up to several atom units by approaching a tip to surface within several angstroms. When the tip approaches to the surface of the sample, interaction between atoms that are in the tip and other atoms in the sample occurs. The magnitude of interaction force is usually as strong

as Van der Waals force which is weak as 10^{-9} N. However, this weak power affects the resonance frequency or bending degree of the tip and this change is measured by the laser.

The surface morphology of the etched specimen was measured by AFM as shown in Fig. 4-2. The surface of wet etched area (dark brown area) was rather smooth and RMS value of 1.544 nm was obtained when the etching time was 200 s. The RMS values of etched area were similar regardless of etching time difference. Non-etched area shows RMS value of 1.620 nm. AFM measurement shows that KOH wet etching result in smooth surface.

4.3.2. Recessed depth as etching time and the uniformity

Figure 4-3 shows the measured recessed-depth versus wet etching time. The value in the graph is the average value of randomly selected ten samples not just one sample to guarantee the uniformity. From 0 s to 150 s, the recess-depth increased linearly as time passes. The etching rate of 0.153 nm/s was measured.

However, the recess-depth was not increased after 150 s wet etching. The value of recess-depth was 23 nm which is the sum of the GaN cap layer (3 nm) and AlGaN barrier layer (20 nm). This wet etching result indicates that AlN can be employed as an etch stopper when AlGaN/Gan HEMT is applying KOH wet etch for the gate-recessed structure. So to speak, I can guarantee the KOH wet etching uniformity by high etching selective characteristic of AlN.

In order to investigate the uniformity of the KOH wet etching, I measured V_{TH} of all fabricated devices. Figure 4-4 exhibits a histogram of V_{TH} for all 26 fabricated AlGaN/GaN MOS HEMTs. As you can see in the graph, the range of the variation is about 1 V for each etching time (non-etched, 100 s etched, 200 s etched). This result also indicates the KOH wet etching without any additional activation treatment also has a good uniform etching characteristic.

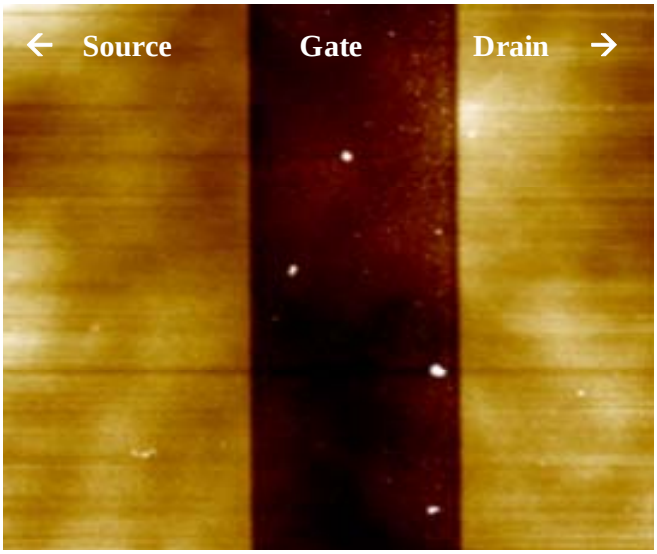

(a)

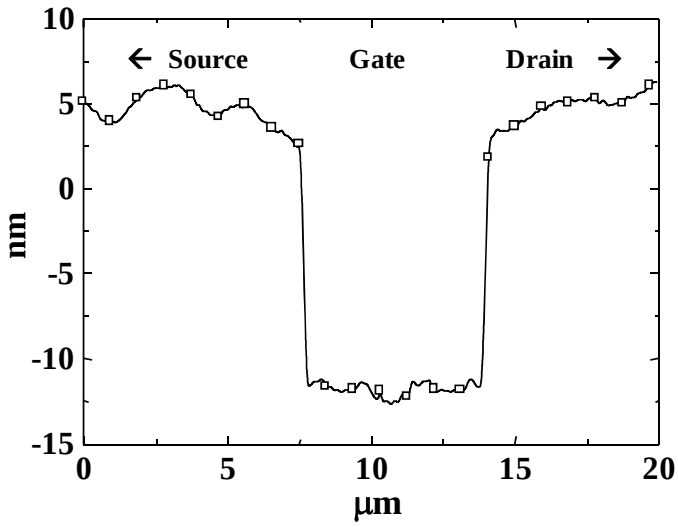

(b)

Figure 4-2: The AFM image of after wet etching of AlGaN/GaN specimen **(a)** the etched surface **(b)** the cross-sectional view of KOH etched sample

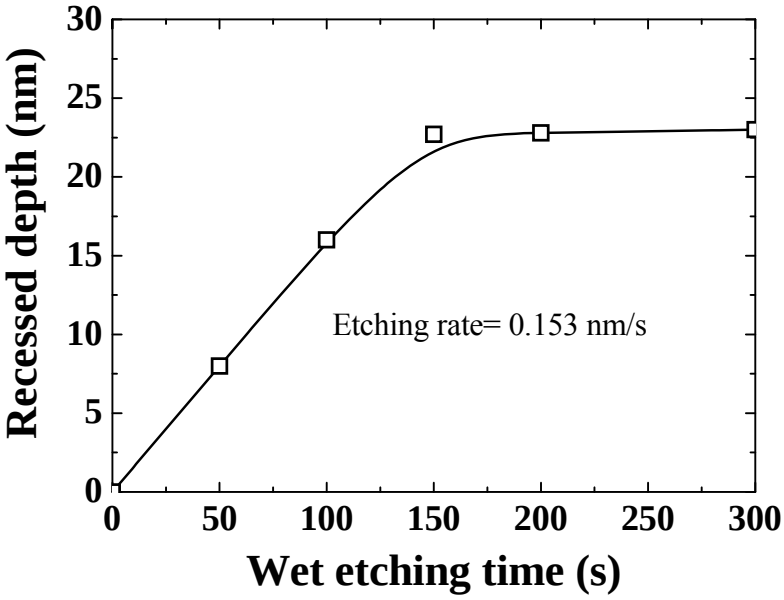

Figure 4-3: The recessed depth of AlGaN/ GaN specimen versus etching time

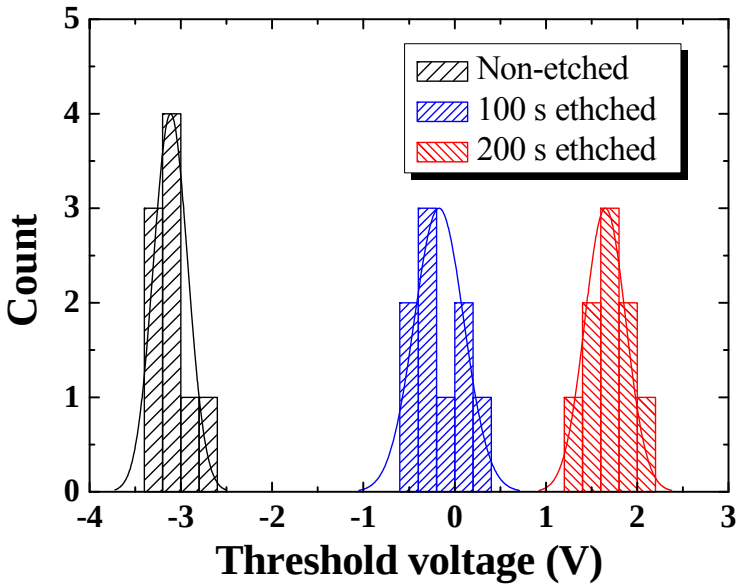

Figure 4-4: The histogram of measured threshold voltage of all fabricated devices

4.4. Electrical Properties of Fabricated AlGaN/GaN MOS HEMTs

4.4.1. Forward Characteristics

As you can see in Fig. 4-5, as etching time increases, V_{TH} shifts to the positive direction. The V_{TH} of the non-etched device is –3.06 V. As etching time increases, V_{TH} also increases linearly; –1.90 (50 s), –0.25 (100 s), and 1.50 V (150 s), respectively. The V_{TH} of the device with 200 s etching time exhibits almost identical result with that of 150 s etched device because of saturated recessed depth. This result also indicates that the KOH wet etch has high etching selectivity between AlGaN and AlN layers.

Recessed AlGaN under the gate region may induce relatively low 2DEG so that bring about a lower drain current. Thus I measured the DC output characteristics for non-etched and recessed-gate AlGaN/GaN HEMTs as shown in Fig. 4–6. Compared to the non-etched HEMT with $I_{D,max}$ > 210 mA/mm at V_{GS}= 0 V, recessed-gate HEMT shows small $I_{D,max}$ of 90 mA/mm at V_{GS}= 4 V. The $R_{on,\ sp}$ (on-resistance) of 8.36 mΩ·cm^2 for the recessed-gate HEMT etched for 200 s is larger than that of non-etched HEMT (5.260 mΩ·cm^2). High $R_{on,\ sp}$ and low $I_{D,max}$ may be attributed to the higher resistance near the recessed gate region.

4.4.2. Drain leakage current Characteristics

Figure 4-7 (a) shows the drain leakage current characteristic of non-

etched and gate-recessed MOS HEMTs at V_{GS} of –10 V. The leakage current characteristics are considerably improved by applying HfO_2 as gate insulator. Both non-etched and gate recessed MOS HEMTs exhibited the leakage current lower than 3 nA/mm. These results indicate that the RF-sputtered HfO_2 is useful to improve the surface problems such as leakage current and electron trapping by passivating the GaN surface.

Also, in order to investigate the stable operation at normally-off condition, I measured the drain leakage current when the gate voltage is 0 volt. As you can see in Fig.4-7 (b), the leakage current of the device was somewhat increased by reduced depletion region due to the increase of applied gate voltage. However, still both 150 s etched and 200 s etched sample exhibits the leakage current less than 0.5 μA/mm. Considering 1mA/mm is the general turn-on condition for semiconductor devices, the fabricated AlGaN/GaN MOS HEMT is successfully operating even in the normally-off condition.

4.4.3. Breakdown Voltage Characteristics

Figure 4-8 (a) shows the breakdown voltage of non-etched and gate-recessed MOS HEMTs. The breakdown voltage was defined at the leakage current of 1 mA/mm and measured when V_{GS} is –5 V. The breakdown voltage of conventional device without HfO_2 gate insulator was only 600 V. However, the breakdown voltage of both non-etched and gate-recessed devices exhibited about 1600 V by applying HfO_2 as a gate insulator. Only 200 s etched device showed marginal degradation of the breakdown voltage. The breakdown voltage of AlGaN/GaN HEMTs is determined by

electron runaway on the surface [50]. The injected electrons from the gate into the surface states lead to surface leakage current in the conventional HEMT. In the proposed MOS-HEMT, the trap-assisted Schottky tunneling current and the surface leakage current caused by electrons trapping are successfully suppressed by the RF-sputtered HfO_2 gate insulator such that the device with HfO_2 sustains a high breakdown voltage.

As I investigated the drain leakage current at the normally-off condition in section 4.4.3., I also measured breakdown voltage of fabricated devices in the case of the V_{GS} is 0 V. As you can see in Fig. 4-8 (b), even though the breakdown voltage somewhat decreased when the V_{GS} is 0 V, still both 150 s etched and 200 s etched sample showed the breakdown voltage more than 1200 V.

4.4.4. Capacitance-Voltage Characteristics

Figure 4-9 shows capacitance-voltage (C-V) characteristics of 100 s and 200 s etched gate recessed AlGaN/GaN MOS-HEMTs. The frequency was 1 MHz and V_{GS} was swept from –10 to 5 V. In the case of the 100 s etched device, considerable hysteresis of 1 V near V_{TH} was investigated. However, in the case of 200 s etched device, a relatively small hysteresis 0.3 V was investigated. This result indicates the existence of acceptor-like traps at the interface between HfO_2 and the surface of remained AlGaN barrier layer in the case of 100 s etched device. Also, at the positive gate bias, 200 s etched device showed relatively small capacitance value than that of 100 s etched device. This is because the absent of AlGaN barrier layer in the case of 200 s etched device.

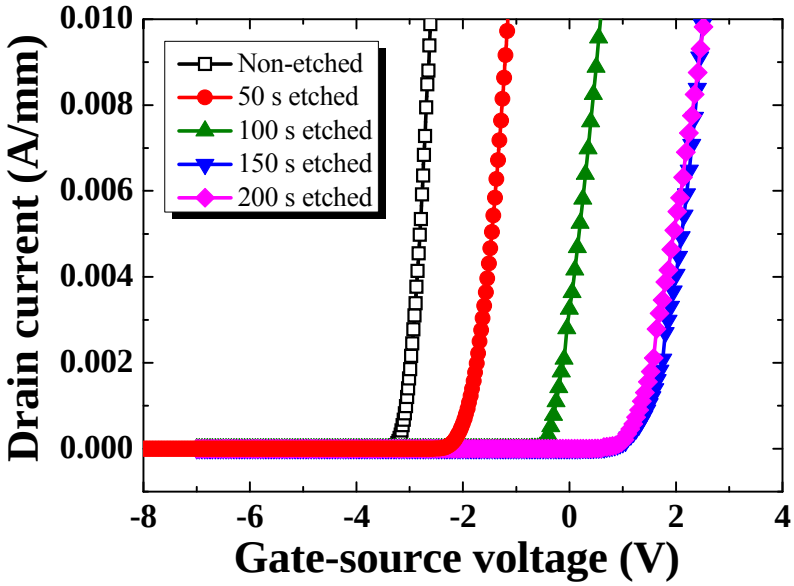

Figure 4-5: Comparison of threshold voltage of non-etched and gate-recessed MOS HEMTs

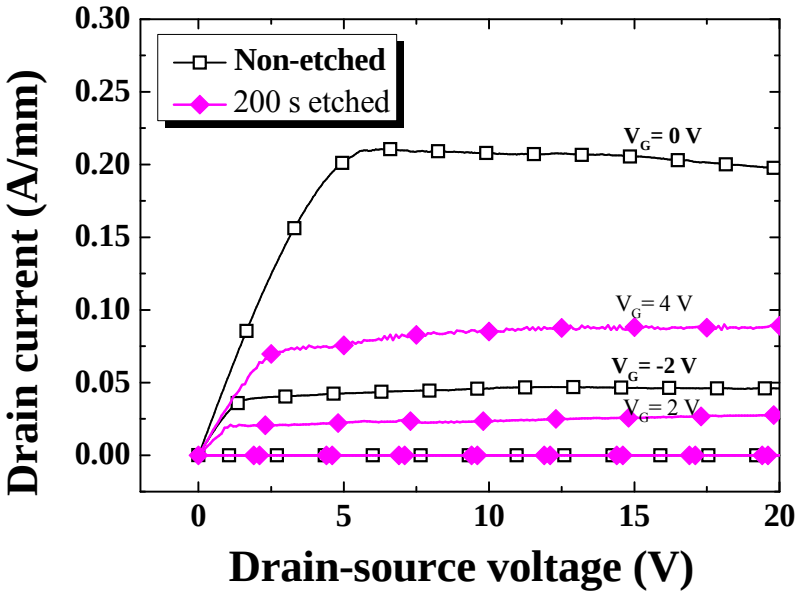

Figure 4-6: DC output characteristics of non-etched and gate-recessed MOS HEMTs

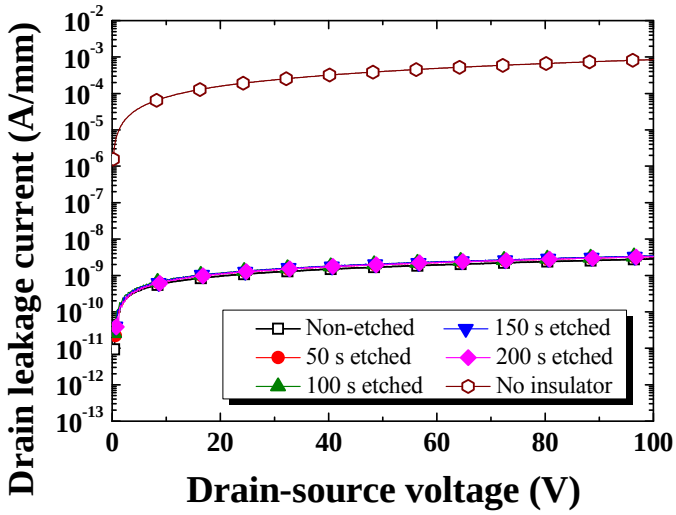

(a)

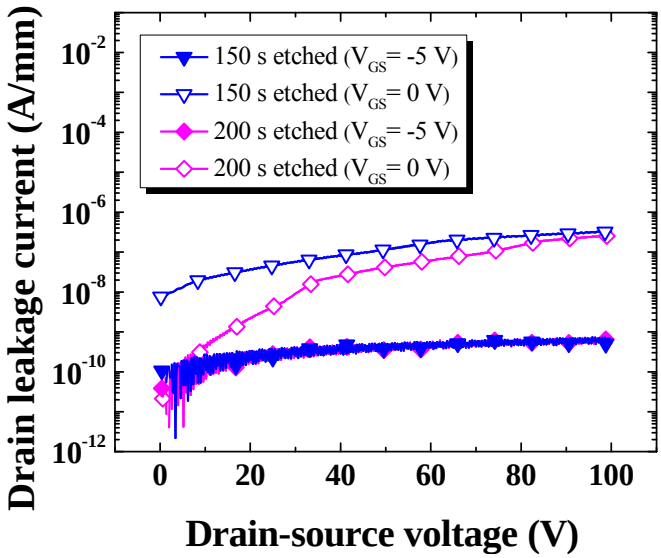

(b)

Figure 4-7: Drain leakage current characteristics of non-etched and gate-

recessed MOS HEMTs

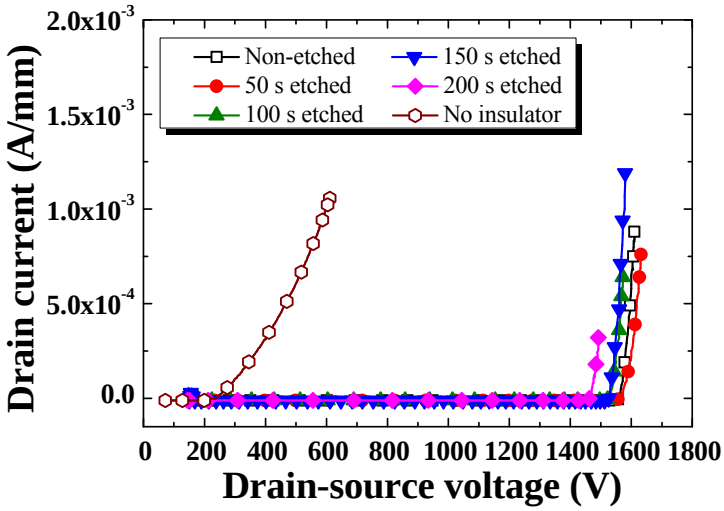

(a)

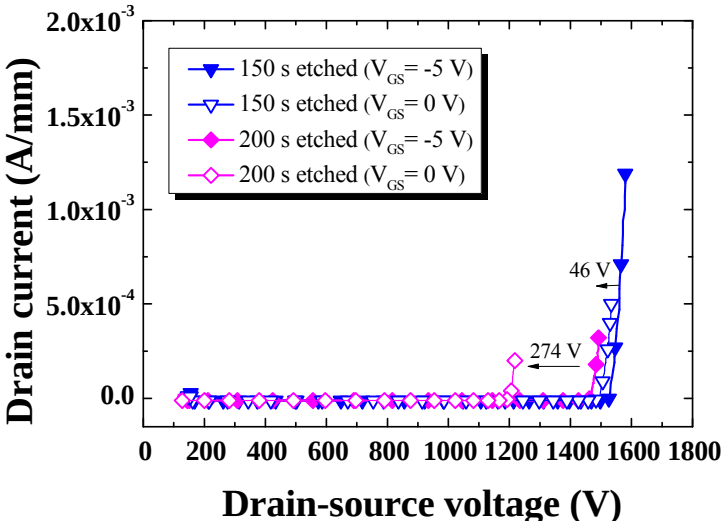

(b)

Figure 4-8: Breakdown voltage of non-etched MOS HEMT and gate-recessed MOS HEMTs

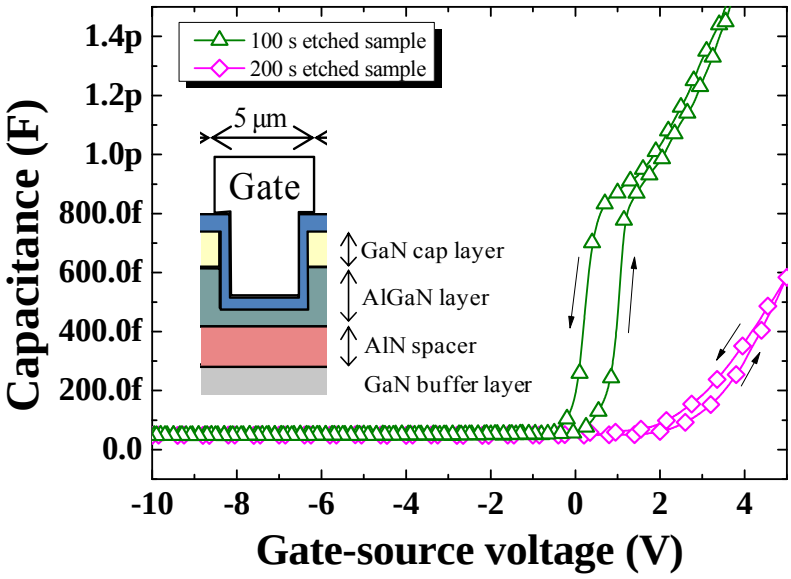

Figure 4-9: *C-V* characteristics of the 100 s and 200 s etched AlGaN/GaN MOS-HEMTs

4.5. Summary

I have successfully fabricated normally-off AlGaN/GaN MOS HEMTs by simple KOH wet etching technique to fabricate recessed-gate structure and RF sputtered HfO_2 as a gate insulator. The proposed KOH wet etching exhibited an uniform recess-depth and smooth etched surface. V_{TH} of the gate-recessed HEMT shifted from –3 to 1.5 V after 150 s KOH-wet etch. Also, the RF-sputtered HfO_2 gate insulator successfully suppressed the leakage current by blocking the gate leakage current and passivating the GaN surface. The breakdown voltage and $R_{on,\ sp}$ was 1580 V and 8.089 mΩ·cm^2, respectively. It corresponds to a figure of merit ($BV^2/R_{on,\ sp}$) of 308 MW/cm^2. My experimental results show that the proposed KOH wet etching and RF sputtered HfO_2 may be a promising method for the fabrication of normally-off AlGaN/GaN MOS HEMTs.

Chapter 5

5. Conclusion and Future Works

In this thesis, AlGaN/GaN HEMTs employing H_2O annealing and RF-sputtered HfO_2 as a gate insulator are presented and also the results of simple KOH wet etching is described. Both H_2O annealing and RF-sputtered HfO_2 improved the reverse blocking characteristics of AlGAN/GaN HEMTs. Also, simple KOH wet etching without any additional treatment realized uniform and reliable recessed-depth so that high-performance normally-off AlGaN/GaN MOS-HEMTs were successfully fabricated.

O_2 annealing has been widely used to increase the reverse blocking characteristics of AlGaN/GaN HEMTs. This method forms thermally oxidized GaO_X layer on the GaN surface so that electrons from the gate will be trapped by Ga vacancies in the GaO_X layer. Eventually, by removing electrons at the surface, the leakage current will be suppressed. The principle of H_2O annealing is also similar to O_2 annealing. However, I

expected more efficient formation of GaO_X layer due to its smaller molecule size and the result was confirmed by XPS and AES measurement. Moreover, the electrical characteristics of AlGaN/GaN HEMTs employing H_2O annealing showed better results than that of O_2 annealing. The breakdown voltage and drain leakage current of AlGaN/GaN HEMT employing the H_2O annealing treatment were 1674 V and 13.1 nA/mm, while those values with the O_2 treatment were 1512 V and 60.1 nA/mm. However, pulsed *I-V* characteristic of the devices was degraded due to deep traps in GaO_X on the surface of the device. As a result, I could realize that the H_2O annealing is not an appropriate treatment for the RF application even though it improves reverse blocking characteristic of AlGaN/GaN HEMTs.

Next, I proposed AlGaN/GaN MOS-HEMTs employing RF-sputtered HfO_2 gate insulator and KOH wet etching for the gate-recessed structure. Unlike H_2O annealing treatment, I confirmed enhanced pulsed *I-V* characteristic when I applied RF-sputtered HfO_2 to the device. Also, weak crystallizability of HfO_2 was investigated even when the material is deposited by the sputtering method. Sputtering method is widely known as a very advantageous deposition method for its simplicity, high through put and low cost. In addition, for the normally-off operation, I adopted simple KOH wet etching without any catalytic treatment at room temperature. It is well known that the Ga-face GaN is hardly etched in the KOH solution. However, I investigated uniform and reliable recess-depth of the etched sample by AFM measurement. By employing RF-sputtered HfO_2 gate insulator and simple KOH wet etching, I could fabricate high-performance normally-off AlGaN/GaN MOS HEMTs exceeding figure of merit (FOM) value of 308 MW/cm^2 and V_{TH} of 1.5 V.

However, further research of KOH wet etching mechanism must be carried on. Even though an uniform and reliable etching results were obtained in the same wafer, the recess-depth was different in the case of another wafer deposited by other wafer companies. Also, to improve the quality of RF-sputtered HfO_2 gate insulator, further research about the HfO_2 sputtering conditions, post annealing for crystallization of HfO_2 and interface characteristic between GaN and HfO_2 must be done.

Appendix

Appendix. Au-Free AlGaN/GaN MOS-HEMTs

A. Overview

Another important issue for AlGaN/GaN device is Au-free fabrication issue. In order to make AlGaN/GaN devices commercially available, AlGaN/GaN devices fabrication on Si wafers with diameter of 6 inches so called GaN-on-Si wafers is now actively under investigation. This Au-free process for AlGaN/GaN device will enables the fabrication of GaN high voltage transistor in many 6-inch CMOS fabs and eventually will reduce the cost of products considerably. Of all the most, the Au-free GaN devices have also been attracted due to the high cost of Au. Thus, Au-free issue is an inevitable issue which must be overcome and already many groups have reported Au-free GaN devices [51-54].

The purpose of this chapter is to propose Au-free fabrication process for AlGaN/GaN devices. In appendix B, I compared two CMOS-compatible metals such as Cu and W with Au. I successfully fabricated and investigated AlGaN/GaN HEMTs employing Cu and W as a conducting metal.

Also, in appendix C, I compared conventional Ni based Schottky contact with sputtered TaN and Indium-tin-oxide (ITO) for Au-free fabrication process and rather good reverse blocking characteristic. I selected TaN and ITO for the replacement material since TaN is stable at high temperature and an inoxidizable ceramic material so that TaN is a suitable material for Schottky metal in AlGaN/GaN SBDs [55]. Also, ITO has been widely employed to many opto-electronic devices for its highly conductive, good adherence to many substrates, and good transmission characteristic properties [56]. At last, I fabricated and figured out rather stable various Schottky contact by employing TaN and ITO for AlGaN/GaN SBDs by RF-sputtering without Au layer.

B. Comparison between Ni/Au with Ni/Cu and Ni/W contact

To date, Au has been widely employed as a contact metal for AlGaN/GaN HEMTs due to its low resistivity and inertness to most wet chemicals [57]. However, Au is an inappropriate metal in Si-fab because of its contamination issue. In addition, in the case of long-term device operation, gold diffusion has been investigated as a crucial reason for the Ohmic contact degradation [58]. Thus, the necessity of CMOS-compatible metal for AlGaN/GaN HEMTs has been brought up as an important issue recently.

In this chapter, I compared conventional Ni/Au based contact with Ni/Cu and Ni/W contact. Copper (Cu) has been widely employed as an interconnect metals in conventional Si devices. Due to its low resistivity characteristic and cheaper cost than Au, Cu is a promising metal for the GaN HEMT conducting and interconnection. Also, tungsten (W) is another good conducting metal due to its low resistivity and stable characteristic even in high temperature. Both Ni/Cu and Ni/W were deposited by same method and the electrical characteristics of fabricated devices are exhibited.

B.1. Device Fabrication

The cross-sectional view of the fabricated device is shown in the Fig. B-1. AlGaN/GaN hetero-structure was grown on Si (111) substrate. The structure grown by metal-organic chemical vapor deposition comprises the following specific layers: the nucleation layer, a 3.9-μm-thick C-doped GaN buffer layer, a 100-nm-thick unintentionally-doped (UID) GaN layer, a 20-nm-thick UID-$Al_{0.23}Ga_{0.77}N$ barrier layer, and a 3-nm-thick UID-GaN cap layer. Mesa isolation using Cl_2 based ICP-RIE was performed in order to define an active region. Ohmic metals of Ti/Al/Ni/Au (20/80/20/100 nm) for source and drain was formed by e-gun evaporation. At the same time, I made other Ohmic metal samples which replaced Au with Cu and W (100 nm), respectively. Both Cu and W were deposited by e-gun evaporation. After forming Ohmic contact, I deposited 15 nm thickness of sputtered HfO_2 for the gate insulator and passivation effect. Lastly, I formed Schottky metals of Ni/Au, Ni/Cu, and Ni/W (30/150 nm), respectively, for the gate electrode. The gate length, gate-drain distance, and gate width were 3, 20, and 50 μm, respectively.

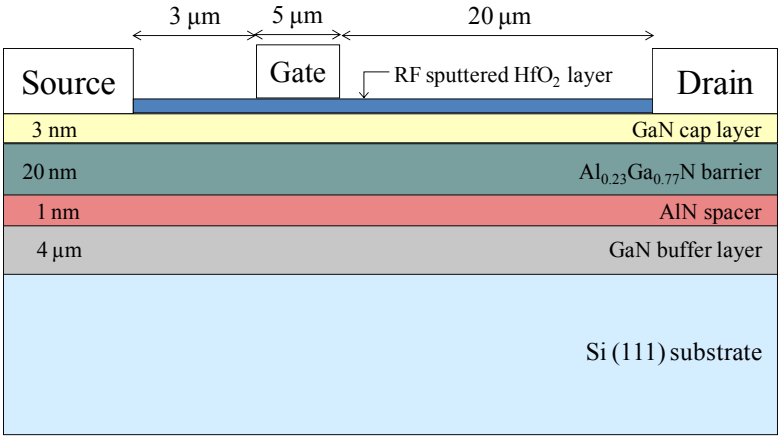

Figure B-1: Cross-sectional view of fabricated devices

B.2. DC Output Current Characteristics

Figure B-2 (a) shows the DC characteristics of three kinds of unit cell device for comparison. Compared to the Au device (I_D of 0.28 A/mm at V_{DS}= 20 V), Cu device shows I_D of 0.25 A/mm which is 90 % current level that of Au device. However, the W sample shows I_D of 0.10 A/mm which is only 36 % current level that of Au sample. Considering lower resistivity of Cu than that of Au, reduced DC on current may caused by contact. In order to confirm the reason for reducement of DC current degradation in the case of Cu and W, I measured contact resistance by TLM method. The contact resistance value of Ni/Au contact was 0.59 Ω·mm whereas Ni/Cu and Ni/W was 10.76 Ω·mm and 117.77 Ω·mm, respectively. Considerably high contact resistance was the reason for DC on current degradation. Thus, further research about the Ohmic contact annealing condition for each Cu and W device will be required.

Figure B-2 (b) shows the DC characteristics of multi-cells employed various conducting metal; Au, Cu, and W. Almost equal current level of Au and Cu device was exhibited. This results indicate that in the case of multi-cells, the effect of high contact resistance to current level is marginal. By depositing Cu thicker, much higher current level than that of Au device were measured. The higher current level may attributed to low resistance along with electrodes due to thicker thickness of the electrode.

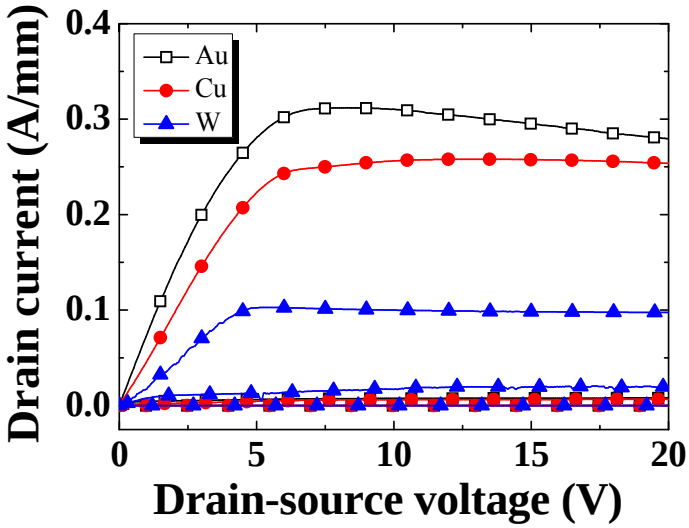

(a)

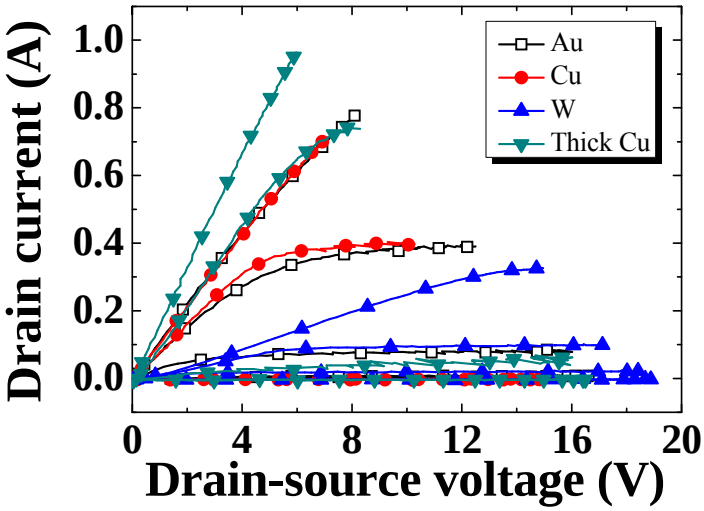

(b)

Figure B-2: DC output characteristic of **(a)** Unit cell device **(b)** Multi-cells

B.3. Reverse Blocking Characteristics

The reverse blocking characteristics of Au, Cu, and W device are shown in Fig. B-3 (a) and Fig. B-3 (b). Measured devices had a gate length of 5 μm, gate-source distance of 2 μm, and gate-drain distance of 15 μm. All devices have a similar gate leakage current of < 100 pA/mm, drain leakage current of < 500 pA/mm, and three-terminal breakdown voltage of ~ 1600 V. In contrast with forward characteristics, reverse blocking characteristics of all Ni/Au, Ni/Cu, and Ni/W exhibit stable characteristics. To sum up, no degradation of reverse blocking characteristics was investigated in the case of Ni/Cu and Ni/W contacts.

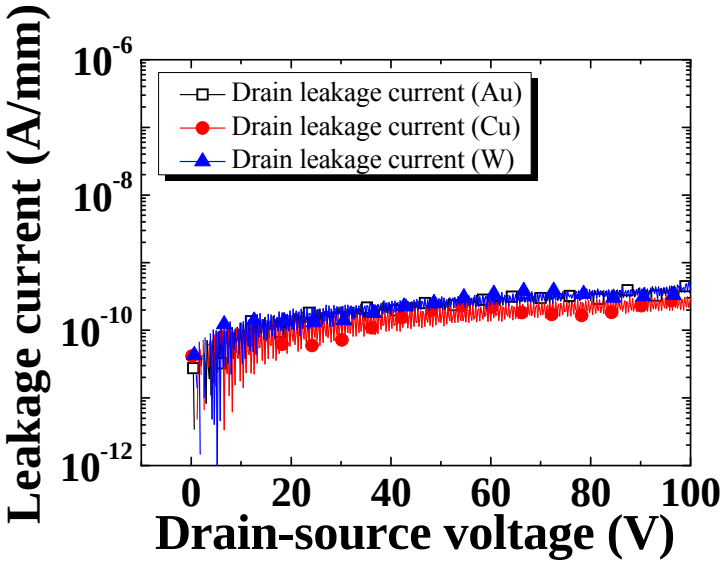

(a)

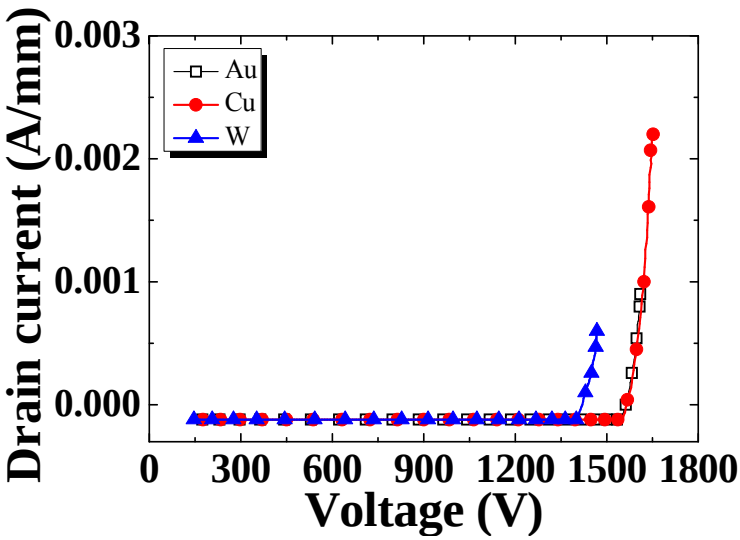

(b)

Figure B-3: Reverse blocking characteristics of fabricated devices **(a)** Drain leakage current **(b)** Breakdown voltage

B.4. Summary

I compared various conducting metals such as Au, Cu, and W for the electrode of AlGaN/GaN HEMTs. All devices showed similar reverse blocking characteristics. However, the forward characteristics of Au and Cu devices were better than that of W device. If I employed thicker Cu electrode, Cu devices exhibited better device performance than that of Au devices. In conclusion, once the Ohmic annealing condition of Ni/Cu and Ni/W is optimized, these two metals will be a promising metal for AlGaN/GaN devices‘ electrode and interconnection instead of gold.

C. Sputtered Schottky Contact for Au-free AlGaN/GaN Devices

With Au-free issue, Ni based Schottky metals issue has been brought up recently too. Ni based Schottky metals have been widely employed for an anode electrode of AlGaN/GaN devices due to a high work function and a good adhesion with GaN materials. However, Ni is easily oxidized so that thick Au on the Ni is required and it is rather difficult to form a thick Ni electrode because of strong internal stress [57, 59]. Moreover, metal based Schottky contact may not be stable during the high current and high temperature operation due to the inter-diffusion between metal and AlGaN/GaN heterostructure by slight melting [60]. A rather stable Schottky metal contact is desired even under the harsh environment.

C.1. Device Fabrication

The cross-sectional view and top view of the proposed device are shown in Fig. C-1. AlGaN/GaN heterostructure was grown on Si (111) substrate by metal-organic chemical vapor deposition. The structure comprises the following specific layers; 3.9 μm-thick C-doped GaN buffer layer, 100 nm-thick i-GaN, 30 nm-thick i-$Al_{0.23}Ga_{0.77}N$ barrier layer, and 3 nm-thick i-GaN cap layer. The measured channel electron mobility, sheet carrier concentration, and sheet resistance were 1860 $cm^2/V\cdot s$, 4.34×10^{12} $/cm^2$, and 773 Ω/□ by Hall measurement.

Mesa isolation using Cl_2-based inductively coupled plasma-reactive etching was performed in order to define an active region. Ohmic metals of Ti/Al/Ni/Au (20/80/20/100 nm) for cathode were formed by e-gun evaporation and lift-off. I annealed the ohmic metals at 880 ^oC for 40 s under N_2 ambient. Prior to Schottky contact formation, I dipped the samples into the 30:1 buffered oxide etchant (BOE) for 30 s and diluted HCl (D.I. water : HCl = 5 : 1) for 1 min.

Both TaN and ITO for anode were deposited by sputtering at room temperature and the thickness of TaN was 43 nm and that of ITO was 60 nm. Specific deposition conditions are listed in Table C-1. The conventional device with Ni/Au (30/150 nm) Schottky contact was also fabricated for a comparison purpose.

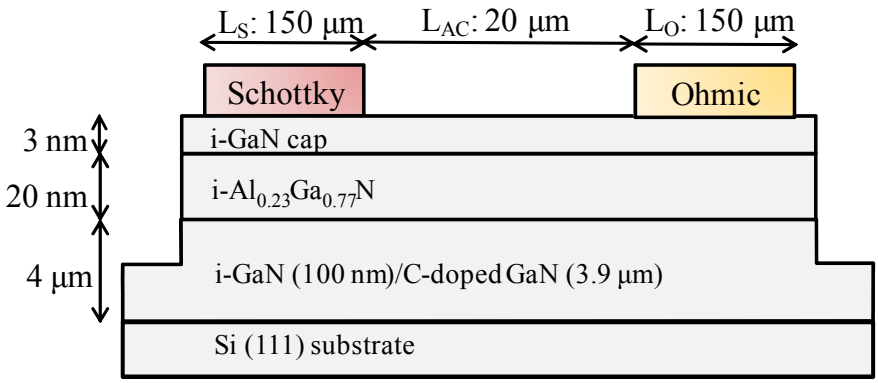

Figure C-1: Cross-sectional view of fabricated SBDs

Table C-1. Specific deposition conditions of sputtering

	TaN	**ITO**
Sputtering power (W)	300 (RF)	300 (DC)
Sputtering pressure (mtorr)	1	3
Temperature	Room temperature	Room temperature
Ar gas flow (sccm)	20	15

C.2. Forward Characteristics

Figure C-2 shows the forward characteristics of the fabricated devices at room temperature. The device of Ni/Au Schottky contact shows forward current of 240.0 mA/mm at 5 V while TaN and ITO Schottky device shows 91.5 mA/mm, and 131.6 mA/mm, respectively. A forward current reduction may be caused by the high Schottky barrier height of contact. Also the higher resistance of TaN (244.3 $\mu\Omega\cdot$cm) and ITO (216.0 $\mu\Omega\cdot$cm) than that of Ni (6.9 $\mu\Omega\cdot$cm) and Au (2.2 $\mu\Omega\cdot$cm) may be attributed to reduction of forward current.

The SBH (Φ_{BN}) of the conventional device and the proposed one were extracted by below equation [61].

$$\Phi_{BN} = \frac{KT}{q}\ln\left(\frac{A^{**}T^2}{J_S}\right)$$

J_S is the saturation current density obtained by *I-V* characteristics at 0 V, A^{**} is the effective Richardson constant assuming 26.64 A·cm^{-2}·K^{-2}, and the temperature is 300 K. The TaN Schottky SBDs has SBH of 0.62 eV and the ITO schottky SBDs has SBH of 0.54 eV. However, the conventional Ni/Au Schottky SBDs exhibits 0.51 eV. As shown in Fig. C-2, due to high SBH, the turn-on voltage of the TaN and ITO Schottky SBDs showed 0.46 V and 0.39 V, respectively. The conventional Ni/Au Schottky SBDs showed turn-on voltage of 0.32 V. High turn-on voltage may not be suitable in a typical power conversion system. However, the difference of turn-on voltage was insignificant and the reverse blocking characteristics of TaN and ITO Schottky SBDs were fairly improved.

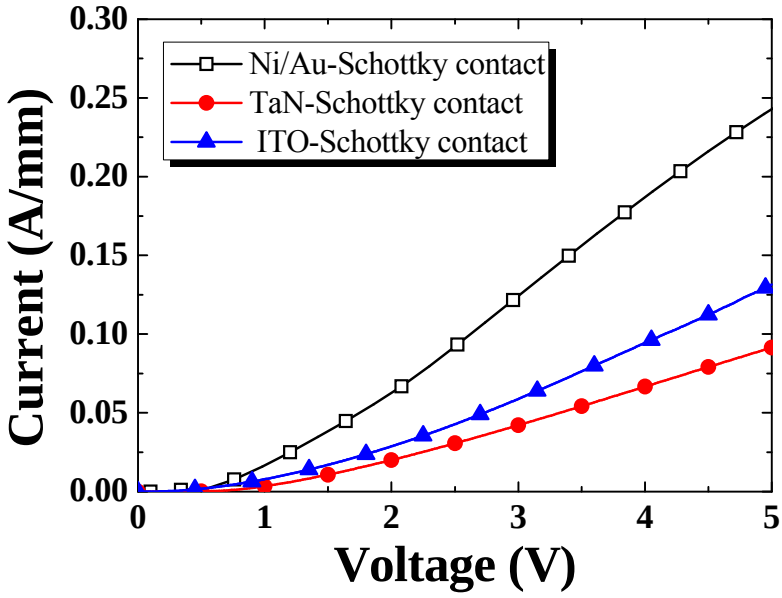

Figure C-2: Transfer characteristic of fabricated devices

C.3. Reverse Blocking Characteristics

Figure C-3 (a) shows the rectifying characteristics of each devices at room temperature. The Ni/Au Schottky device shows high leakage current of 1.55 mA/mm at –100 V due to the amount of surface trap-assited Schottky tunneling current. However, TaN and ITO Schottky device shows decreased leakage current of 111 μA/mm and 530 μA/mm, respectively. The results may indicate that the TaN and ITO Schottky contact shows better stable blocking characteristics than Ni/Au Schottky contact. The stable blocking characteristics may indicate that the TaN and ITO Schottky contact is more suitable to sustain the high voltage than conventional Ni/Au.

As shown in Fig. C-3 (b), I achieved the breakdown voltage of 605 V by using TaN Schottky contact while that of the device with ITO is 472 V. The conventional device exhibited the breakdown voltage of 335 V. This breakdown voltage results are attributed to stable blocking characteristics and high SBH of TaN and ITO Schottky contact. Rather high SBH of TaN and ITO Schottky contact by RF-sputtering indicates that these two materials may be useful to improve reverse blocking characteristics.

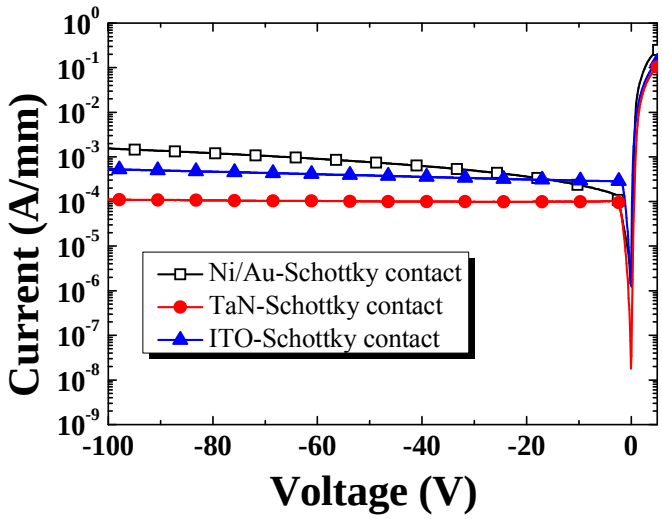

(a)

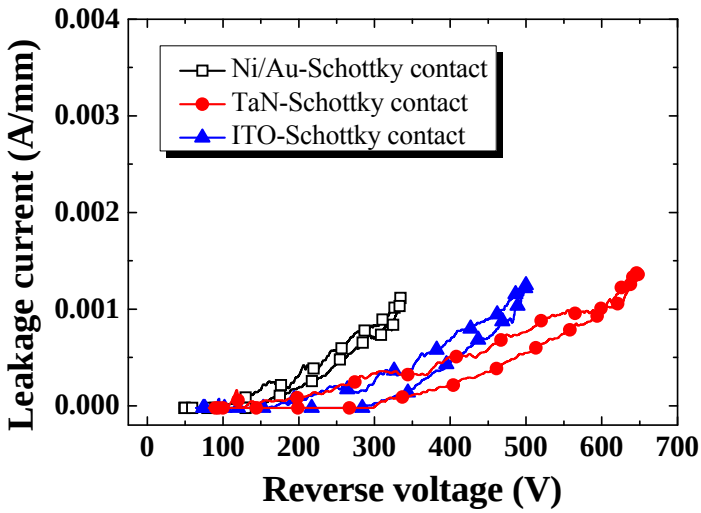

(b)

Figure C-3: Reverse blocking characteristics of fabricated devices **(a)** Leakage current **(b)** Breakdown voltage

C.4. Summary

I proposed and successfully fabricated AlGaN/GaN SBDs employing various Schottky contact by sputtering without Au layer. Even though, the proposed TaN and ITO Schottky contact shows rather decreased forward on current and high turn-on voltage, improved reverse blocking characteristics such as low leakage current and high breakdown voltage compared to Ni/Au schottky contact was investigated. The summary of electrical properties of fabricated various Schottky SBDs are exhibited in the following table. The results show that TaN and ITO deposited by sputtering method may be a suitable anode material and more economical than Ni/Au for high voltage operation in the power AlGaN/GaN SBDs.

References

[1] T. P. Chow and R. Tyagi, "Wide bandgap compound semiconductor for superior high-voltage power devices", in *Proc. Int. Symp. Power Semiconductor and ICs*, 1994, pp. 1481-1483.

[2] International Rectifier, "Commerciallization of GaN based Power Devices: An Introduction to GaNpowIR", 2010.

[3] J. L. Hudgins, G. S. Simin, E. Santi and M. A. Khan, "An assessment of wide bandgap semiconductor for power devices", *IEEE Trans. Power Electronics*, vol. 18, no. 3, pp. 907-914, 2003.

[4] B. S. Kang, F. Ren, Y. Irokawa, K. W. Baik, S. J. Pearton, C. -C. Pan, G. -T. Chen, J. -I. Chyi, H. -J. Ko and H. -Y. Lee, "Temperature dependent characteristics of bulk GaN Schottky rectifiers on free-standing GaN substrates", *J. Vac. Sci. Technol. B*, vol. 22, no. 2, pp. 710-714, 2004.

[5] S. Keller, Y. -F. Wu, G. Parish, N. Ziang, J. J. Xu, B. P. Keller, S. P. DenBaars and U. K. Mishra, "Gallium nitride based high power heterojunction field effect transistors: process development and present status at UCSB", *IEEE Trans. Electron Devices*, vol. 48, no. 3, pp. 552-559, 2001.

[6] R. J. Champbell, and K. Rajashekara, "Evaluation of power devices for automotive hybrid and 42 V based systems", *Delphi Corporation, U. S. A., SAE World Congress, SAE Techninal paper series*, 2004-01-1682, 2004.

[7] M. Ishiko, "Recent R&D Activities of Power Devices for Hybrid Electric Vehicles", Toyota, Japan, *R&D Review of Toyota CRDL*, vol. 39, no. 4, 2004.

[8] K. Hirama, T. Koshiba, K. Yohara, H. Takayanagi, S. Yamaguchi, M. Satoh and H. Kawarada, "RF diamond MISFETs using surface accumulation layer", in *Proc. Int. Symp. Power Semiconductor Device and ICs*, 2006, pp. 1-4.

[9] E. O. Johnson, "Physical limitations on frequency and power parameters of transistors", *RCA Rev.*, vol. 26, pp. 163-177, 1965.

[10] B. J. Baliga, "Semiconductor for high-voltage, vertical channel field effect transistors", *J. Appl. Phys.*, vol. 53, no. 3, pp. 1759-1764, 1985.

[11] I. P. Smorchkova, C. R. Elsass, J. P. Ibbetson, R. Vetury, B. Heying, P. Fini, E. Haus, S. P. DenBaars, J. S. Speck and U. K. Mishra, "Polarization-induced charge and electron mobility in AlGaN/GaN heterostructures grown by plasma-assisted molecular-beam epitaxy", *J. Appl. Phys.*, vol. 86, no. 8, pp. 4520-5426, 1999.

[12] J. P. Ibbetson, P. T. Fini, K. D. Ness, et al., "Polarization effects, surface states, and the source of electrons in AlGaN/GaN heterostructure field effect transistors", *App. Phys. Lett.*, vol. 77, no. 2, pp. 250-252, 2000.

[13] S. M. Hurrbard, "Metalorganic vapor phase peitaxy (MOVPE) Growth and Characterization of III-Nitride Heterostructures for Application in Electronic Devices", Ph. D. Dissertation, Department of Electrical Engineering, University of Michigan, 2005.

[14] Transphorm, "http://powerelectronics.com/power-electronics-systems/ apec-2013-new-product-introductions", 2013. [Online].

[15] B. De Jaeger, M. Van Hove, D. Wellekens, X. Kang, H. Liang, G. Mannaert, K. Geens and S. Decoutere, "Au-free CMOS-compatible AlGaN/GaN HEMT processing on 200 mm Si substrates", in *Proc. Int. Symp. Power Semiconductor Devices and ICs*, 2012, pp. 49-52.

[16] D. Disney, H. Nie, A. Edward, D. Bour, H. Shah, and I. C. Kizilyalli, "Vertical Power Diodes in Bulk GaN", in *Proc. Int. Symp. Power Semiconductor and ICs*, 2013, pp. 59-62.

[17] C.-J. Chen, S. Keller, G. Parish, R. Ventury, P. Kozodoy, E. K. Hu, S. P. Denbaars, U. K. Mishra, and Y. Wu, "High-transconductance self-aligned AlGaN/GaN modulation-doped field-effect transistors with regrown ohmic contacts", *Appl. Phys. Lett.*, vol. 73, no. 21, pp. 3147-3149, 1998.

[18] L. Wang, F. M. Mohammed, and I. Adesida, "Dislocation-induced nonuniform interfacial reactions of Ti/Al/Mo/Au ohmic contacts on AlGaN/GaN heterostructure", *Appl. Phys. Lett.*, vol. 87, pp. 14195, 2005.

[19] N. Miura, T. Nanjo, M. Suita, T. Oishi, Y. Abe, T. Ozeki, H. Ishikawa, T. Egawa, and T. Jimbo, "Thermal annealing effects on Ni/Au based Schottky contacts on n-GaN and AlGaN/GaN with insertion of high work function metal", *Solid-State Electron.*, vol. 48, no. 5, pp. 689-695, 2004.

[20] S.-C. Lee, J. Lim, M.-W. Ha, J.-C. Her, C.-M. Yun, and M.-K. Han, "High performance AlGaN/GaN HEMT switches employing 500 ^{o}C oxidized Ni/Au gate for very low leakage current and improvemnet of uniformity", in *Proc. Int. Symp. Power Semiconductor Device and ICs*, 2006, pp. 1-4.

[21] N.-Q. Zhang, S. Keller, G. Parish, S. Heikman, S. P. DenBaars, and U. K. Mishra, "High breakdown GaN HEMT with overlapping gate structure", *IEEE Electron Device Lett.*, vol. 21, no. 9, pp. 421-423, 2000.

[22] J. W. Johnson, A. P. Zhang, W.-B. Luo, F. Ren, S. J. Pearton, S. S. Park, Y. J. Park, and J.-I. Chyi, "Breakdown voltage and reverse recovery characteristics of free-standing GaN Schottky rectifiers", *IEEE Trans.*

Electron. Devices, vol. 49, no. 1, pp. 32-36, 2002.

[23] W.-K. Wang, C.-H. Lin, P.-C. Lin, C.-K. Lin, F.-H. Huang, Y.-J. Chan, G.-T. Chen, and J.-I. Chyi, "Low-k BCB passivation on AlGaN/GaN HEMT fabrication", *IEEE Electron Device Lett.*, vol. 25, no. 12, pp. 763-765, 2004.

[24] M. D. Hampson, S.-C. Shen, R. S. Schwindt, R. K. Price, U. Chowdhury, M. M. Wong, T. G. Zhu, D. Yoo, R. D. Dupuis, and M. Feng, "Polyimide passivated AlGaN/GaN HFETs with 7.65 W/mm at 18 GHz", *IEEE Electron Device Lett.*, vol. 25, no. 5, pp. 238-240, 2004.

[25] O. Ambacher, B. Foutz, J. Smart, J. R. Shealy, N.G. Weimann, K. chu, M. Murphy, A. J. sierakowski, W. J. Schaff, L. F. Eastman, R. Dimitrov, A. Mitchell, and M. Stutzmann, "Two dimensional electron gases induced by spontaneous and piezoelectric polarization in undoped and doped AlGaN/GaN heterostructures", *J. Appl. Phys.*, vol. 87, no. 1, pp. 334-344, 2000.

[26] B. M. Green, K. K. Chu, E. M. Chumbes, J. A. Smart, J. R. Shealy, and L. F. Eastman, "The effect of surface passivation on the microwave characteristics of undoped AlGaN/GaN HEMTs", *IEEE Electron. Device Lett.*, vol. 21, no. 6, pp. 268-270, 2000.

[27] H. Kim, J. Lee, W. Lu, "Gate current leakage and breakdown mechanism in unpassivated AlGaN/GaN high electron mobility transistors by post-gate annealing", *Appl. Phys. Lett.*, vol. 86, pp. 143505-1~143505-3, 2005.

[28] S. Karmalkar, U. K. Mishra, "Enhancement of breakdown voltage in AlGaN/GaN high electron mobility transistors using a field plate", *Electron Devices, IEEE Transactions on*, vol. 48, no. 8, pp. 1515-1521, 2001.

[29] C. Wanjun, K.-Y. Wong; K.J. Chen, "Single-Chip Boost Converter Using Monolithically Integrated AlGaN/GaN Lateral Field-Effect Rectifier and Normally Off HEMT", *IEEE Electron Device Lett.*, vol. 30, no. 5, pp. 430-432, 2009.

[30] C. Yong, Z. Yugang, K. J. Chen, M. L. Kei, "High-performance enhancement-mode AlGaN/GaN HEMTs using fluoride-based plasma treatment", *IEEE Electron Device Lett.*, vol. 26, no. 7, pp. 435-437, 2005.

[31] N. Ikeda, J. Li, and S. Yoshiba, "Normally-off operation power AlGaN/GaN HFET", in *Proc. Int. Symp. Power Semiconductor and ICs*, 2004, pp. 369-372.

[32] N. Ketteniss, M. Eickelkamp, A. Noculak, R.. H. Jansen, A. Vescan, "Processing and characterization of recessed-gate AlGaN/GaN HFETs", *Advanced Semiconductor Devices and Microsystems, 2*008, pp. 151-154.

[33] D. A. Stocker, I. D. Goepfert, E. F. Schubert, K. S. Boutros, and J. M. Redwing, "Crystallographic Wet Chemical Etching of p-Type GaN", *J. Electrochem. Soc.*, vol. 147, no. 2, pp. 763-764, 2000.

[34] D. Buttari, S. Heikman, S. Keller, U. K. Mishra, "Digital etching for highly reproducible low damage gate recessing on AlGaN/GaN HEMTs", *High Performance Devices, 2002. Proceedings. IEEE Lester Eastman Conference on*, 2002, pp. 461-469.

[35] J. A. Bardwell, J. B. Webb, H. Tang, J. Fraser, S. Moisa, "Ultraviolet photoenhanced wet etching of GaN in $K_2S_2O_8$ solution", *J. Appl. Phys.*, vol. 89, no. 7, pp. 4142-4149, 2001.

[36] H. Lu, Z. Wu, and I. Bhat, "Photo-assisted anodic etching of Gallium Nitride", *J. Electronchem. Soc.*, vol. 144, no. 1, pp. L8-L11, 1997.

[37] J. A. Bardwell, J. B. Webb, H. Tang, J. Fraser, and S. Moisa, “Ultraviolet photo-enhanced wet etching of GaN in $K_2S_2O_8$ solution”, *J. Appl. Phys.*, vol. 89, no. 7, pp. 4142-4149, 2001.

[38] O. Seok, W. Ahn, M.-K. Han, and M.-W. Ha, "High on/off current ratio AlGaN/GaN MOS-HEMTs employing RF-sputtered HfO_2 gate insulator", *Semicond. Sci. Technol.*, vol. 28, pp. 025001-1~025011-6, 2013.

[39] Y. Ohno, T. Nakao, S. Kishimoto, K. Maezawa, T. Mizutani, "Effects of surface passivation on breakdown of AlGaN/GaN high-electron-mobility transistors", *Appl. Phys. Lett.*, vol. 84, no. 12, pp. 2184-2186, 2004.

[40] Y.-H. Choi, J. Lim, Y.-S. Kim, O. Seok, M.-K. Kim, M.-K. Han, "High voltage AlGaN/GaN High-Electron-Mobility Transistors (HEMTs) employing oxygen annealing", in *Proc. Int. Symp. Power Semiconductor Device and ICs*, 2010, pp. 233-236.

[41] I. G. Donhowe, and O. Fennema, "Water Vapor and Oxygen Permeability of Wax Films", *J. Am. Oil Chem. Soc.*, vol. 70, pp. 867-873, 1993.

[42] E. D. Readinger, S. D. Wolter, D. L. Waltemyer, J. M. Delucca,S. E. Mohney, B. I. Prenitzer, L. A. Giannuzzi, R. J. Molnar, "Wet thermal oxidation of GaN", *J. Electron. Mater.*, vol. 28, no. 3, pp. 257-260, 1999.

[43] J. Oila, J. Kivioja, V. Ranki, K. Saarinen, D. C. Look, R. J. Molnar, S. S. Park, J. Y. Han, "Ga vacancies as dominant intrinsic acceptors in GaN grown by hydride vapor phase epitaxy", *App. Phys. Lett.*, vol. 82, no. 20, pp. 3433-3435, 2003.

[44] N.-Q. Zhang, B. Moran, S. P. DenBaars, U. K. Mishra, X. W. Wang, T. P. Ma, "Effects of surface traps on breakdown voltage and switching

speed of GaN power switching HEMTs", *Technical Digest - Int. Electron Devices Meet. Tech. Dig.*, 2001, pp. 589-592.

[45] H. Kim, J. Lee, D. Liu, and W. Lu, "Gate current leakage and breakdown mechanism in unpassivated AlGaN/GaN high electron mobility transistors by post-gate annealing", *Appl. Phys. Lett.*, vol. 86, pp. 143505-1~143505-3, 2005.

[46] T. Mattila, and R. M. Nieminen, "study of oxygen point defects in GaAs, GaN, and AlN", *Phys. Rev. B*, vol. 54, no. 23, pp. 16676-16682, 1996.

[47] C. Liu, E. F. Chor, L. S. Tan, "Investigation of HfO_2/AlGaN/GaN metal-oxide-semiconductor high electrin mobility transistors", *Appl. Phys, Lett.*, vol. 88, no. 17, pp. 173504, 2006.

[48] J. Shi, L. F. Eastman, X. Xin, M. Pophristic, "High performance AlGaN/GaN power switch with HfO_2 insulation", *Appl. Phys. Lett.*, vol. 95, no. 4, pp. 042103, 2009.

[49] K. Balachander, S. Arulkumaran, H. Ishikawa, K. Baskar, T. Egawa, "Fabrication of AlGaN/GaN double-insulator metal-oxide-semiconductor high-electron-mobility transistors using SiO_2 and SiN as gate insulators", *Phys. Stat. Sol. (a)*, vol. 202, no. 4, pp. R32-R34, 2005.

[50] Z. H. Liu, G. I. Ng, H. Zhou, S. Arulkumaran, Y. K T Maung, "Reduced surface leakage current and trapping effects in AlGaN/GaN high electron mobility transistors on silicon with SiN/Al_2O_3 passivation", *Appl. Phys. Lett.*, vol. 98, no. 11, pp. 113506, 2011.

[51] H.-S. Lee, D. S. Lee, and T. Palacios, "AlGaN/GaN High-Electron-Mobility transistors Fabricated Through a Au-Free Technology", *IEEE Electron Dev. Lett.*, vol. 32, no. 5, pp. 623-625, 2011.

[52] H.-C. Chiu, C.-W. Lin, H.-L. Kao, G.-Y. Lee, J.-I. Chyi, H.-W. Chuang, K.-J. Chang, Y.-T. Gau, "A gold-free fully copper metalized AlGaN/GaN power HEMTs on Si substrate", *Microelectronics Reliability*, vol. 52, pp. 2556-2560, 2012.

[53] B. D. Jaeger, M. V. Hove, D. Wellekens, X. Kang, H. Liang, G. Mannaert, K. Geens, S. Decoutere, "Au-free CMOS-compatible AlGaN/GaN HEMT processing on 200 mm Si substrates", in *Proc. Int.Symp. Power Semiconductor Device and ICs*, 2012, pp. 49-52.

[54] S. Lenci, X. Kang, D. Wellekens, M. V. Hove, S. Boulay, S. Stoffels, K. Geens, M. Zahid, and S. Decoutere, "Au-free, High-Breakdown AlGaN/GaN MISHEMTs with Low Leakage, High Yield and Robust TDDB Characteristics", *CS MANTECH Conference*, pp. 231-234, 2012.

[55] C. S. Kang, H.-J. Cho, Y. H. Kim, R. Choi, Onishi, and A. Shahriar Lee, " Characterization of resistivity and work function of sputtered-TaN film for gate electrode applications", *J. Vac. Sci. Technol. B*, vol. 21, pp. 2026-2028, 2003.

[56] T. Margalith, O. Buchinsky, D. A. Cohen, A. C. Abare, M. Hansen, and S. P. DenBaars, "Indium tin oxide contacts to gallium nitride optoelectronic devices", *Appl. Phys. Lett.*, vol. 74, pp. 3930-3932, 1999.

[57] M. R. Pinnel, H. G.. Tompkins, and D. E. Heath, "Oxidation of Nickel and Nickel-Gold Alloy in Air at 50 ^{o}C - 150 ^{o}C", *J. Electrochem. Soc.*, vol. 126, no. 7, pp. 1274-1281, 1979.

[58] M. Piazza, C. Dua, M. Oualli, E. Morvan, D. Carisetti, and F. Wyczisk, “Degradation of TiAlNiAu as ohmic contact metal for GaN HEMTs”, *Microelectron. Reliab.*, vol. 49, no. 9–11, pp. 1222–1225, 2009.

[59] J. A. Thornton, D. W. Hoffman, "Internal stresses in titanium, nickel, molybdenum, and tantalum films deposited by cylindrical

magnetron sputtering", *J. Vac. Sci. Technol.*, vol. 14, no. 1, pp. 164-168, 1977.

[60] Y.-H. Choi, J. Lim, Y.-S. Kim, and M.-K. Han, "Diffusion Effect between Schottky Metals and AlGaN/GaN Heterostructure during High Temperature Annealing Process", *MRS Proceedings*, vol. 1167, pp. O05-06, 2009.

[61] S. M. Sze, Physics of Semiconductor Devices 2nd ed., pp. 279, (Wiley, New York, 1981).

Abstract in Korean

AlGaN/GaN HEMTs는 넓은 band-gap 특성으로 인한 높은 임계 전계 (3 MV/cm) 그리고 낮은 진성 전하들의 농도 (10^{10} cm^{-3}) 등의 장점으로 RF나 전력 회로 시스템에 적용될 수 있는 차세대 전력반도체로 각광받고 있다. 또한 AlGaN과 GaN의 heterostructure은 높은 전하 농도 (10^{13} cm^{-2})와 높은 이동도 (2000 cm^2/V·s) 특성을 띄는 2DEG 채널을 형성시키고 이는 AlGaN/GaN HEMT가 높은 항복 전압특성을 갖는 동시에 낮은 온-저항 특성을 띄게 한다.

하지만 표면에 흐르는 높은 누설 전류에 인한 낮은 항복전압은 반드시 해결되어야 하는 중요한 이슈이다. AlGaN/GaN HEMTs는 GaN buffer 층과 기판과의 격자 불일치로 인한 전위, 자발 분극 현상으로 야기된 전하들 그리고 plasma 및 열 공정으로 발생된 질소 빈격자점들에 의해 표면에 상당한 양의 표면 트랩이 존재한다. 높은 항복 전압 특성을 갖기 위해서는 이러한 표면에 존재하는 shallow 트랩에 전자들이 축적되는 현상을 막아야 한다.

본인은 AlGaN/GaN HEMTs의 역방향 특성을 향상시키기 위하여 습식 산화를 제안하였고 이 방법을 이용하여 제작한 소자와 기존에 널리 쓰여졌던 건식 산화를 적용한 소자와 전기적 특성을 비교해보았다. 습식 산화를 적용한 AlGaN/GaN HEMT (L_{GD}= 20 μm)의 항복전압과 누설전류는 각각 1674 V와 13.1 nA/mm (V_{DS}= 100 V, V_{GS}= −10 V) 였고 건식 산화를 적용한 소자는 각각 1512 V와 60.1 nA/mm 였다.

역방향 특성 향상뿐만 아니라 normally-on 특성 또한 AlGaN/GaN HEMT의 중요한 문제점으로 다루어져 왔다. 기존에 보고되었던 거의 모든 AlGaN/GaN HEMT들은 AlGaN 층과 GaN 층 사이에 분극 현상에 의해 유도되는 2DEG로 인해 약 -3 V에서 -6 V의 문턱 전압을 보이는 normally-on

소자였다. AlGaN/GaN HEMT가 회로에 적용되기 위해서는 회로 내의 'Burn-out' 현상의 우려가 없고 추가적인 회로를 구성하지 않아도 되는 normally-off 특성을 갖는 AlGaN/GaN HEMT가 이상적이다.

본 논문에서는 간단한 KOH 습식 식각과 RF-sputtering 방식으로 증착한 HfO_2를 게이트 절연막으로 이용하여 normally-off AlGaN/GaN HEMT를 성공적으로 제작하였고 분석하였다. 제안된 KOH 습식 식각은 일정한 식각률을 보여 적당한 깊이로 샘플의 식각이 가능하였고 식각된 후의 샘플 RMS 값은 더 작아지는 것을 확인하였다. 150 초 동안 게이트 부분을 KOH 습식 식각한 HEMT의 경우 문턱 전압은 3 V에서 1.5 V 로 커졌고 L_{GD}가 20 μm인 소자의 경우 항복 전압은 1580 V, $R_{on,sp}$는 8.90 mΩ·cm^2 으로 측정되었다. 그 결과 308 MW/cm^{2}의 높은 FOM 값을 갖는 소자를 제작할 수 있었다. 본인의 실험 결과로 미루어 봤을 때 제안된 KOH 습식 식각과 RF-sputtering 방식으로 증착한 HfO_2 게이트 절연막은 고성능 normally-off AlGaN/GaN HEMT 제작 방법들 중 좋은 방법이 될 것이라고 생각된다.

마지막으로 부록에서는 최근 AlGaN/GaN HEMT의 또 다른 중요한 문제점인 gold-free 문제점에 대해 다루었다. 기존 소자에 널리 적용되어 왔던 Ni/Au 접합을 Ni/Cu와 Ni/W 접합과 비교하였다. 본인의 실험 결과로 미루어 봤을 때 Cu 역시 AlGaN/GaN HEMT의 전도 금속으로서 좋은 대체 물질이 될 것이라고 생각된다. 더 나아가 본인은 sputtering 방식으로 증착한 다양한 Schottky 접합을 이용하여 고성능 AlGaN/GaN SBDs를 제안하고 제작하였다. 누설전류와 항복전압과 같은 역방향 특성은 TaN와 ITO의 높은 SBH으로 인해 향상되었다. 그러나 TaN과 ITO의 정방향 특성은 기존의 Ni/Au 접합보다는 다소 감소되었다. TaN Schottky SBD의 항복전압은 605 V였고 ITO는 472 V 로써 비교적 높은 수치로 측정되었다. 반면에 Ni/Au Schottky 접합 SBD의 항복전압은 335 V 으로 다소 낮게 측정되었다.

주요어: GaN, AlGaN, Normally-off, 높은 전자 이동도 트랜지스터, 습식 산화, HfO_2, KOH 습식 식각

학 번: 2011-23366